***Organic acid-assisted thermal dehalogenation of halide salt nuclear wastes: From waste salts to borosilicate glass***

Jared M. Oshiro,[(a),*] Hannah Hallikainen,[(b),*] Brian J. Riley,[(a),†] Xiaonan Lu,[(a)] Bhargav Iyer,[(b)] Bryn Merrill,[(b)] Vitaliy Goncharov,[(b)] Jessica M. Westman[(a)], Martin Liezers[(a)], Jaime L. George[(a)], Benjamin Parruzot, [(a)] Jonathan S. Evarts,[(a)] John D. Vienna[(a)] John S. McCloy,[(b)] and Xiaofeng Guo[(b),†]

[(a)]*Pacific Northwest National Laboratory, Richland, WA (USA)*

[(b)]*Washington State University, Pullman, WA (USA)*

*Keywords: dehalogenation; nuclear waste immobilization; nuclear salt wastes; pyroprocessing; molten salt reactors*

## Abstract

Only a handful of high-halide salt waste forms have been demonstrated for vitrification-based immobilization strategies for halide-salt nuclear waste streams (e.g., pyroprocessing wastes, molten salt reactor wastes) and they all have low waste loading potential as well as low chemical durability for high-alkali streams. An alternative approach to direct salt immobilization is salt partitioning prior to waste form fabrication and one option for partitioning is halide removal, called *dehalogenation*. Removing the halogen fraction through dehalogenation can significantly reduce the waste volume required for disposal in the primary waste form. When dehalogenation is performed using organic acids, the dehalogenation reagent can decompose during high-temperature vitrification, reducing waste loading limitations in the waste form. In the current work, different organic acids (i.e., oxalic, formic, acetic, oxamic, and citric) were evaluated for dehalogenation efficiency of a simple chloride salt simulant (7.19% $LaCl_3$, 53.77% LiCl, and 39.04% KCl, by mole) and a more complex chloride salt simulant called ERV3 (electrorefiner version 3) at 150°C–300°C and using $H^+$:$Cl^-$ molar ratios of 1:1, 2:1, and 3:1. Additionally, a borosilicate glass waste form called TARS (or The Average of Refined Specifications) was formulated and characterized for dehalogenated ERV3.

---

* These authors contributed equally to this work
† Corresponding Authors: brian.riley@pnnl.gov (509)372-4651, x.guo@wsu.edu (509)335-7439

## 1 Introduction

Halide salt-based nuclear wastes have been generated from different processes including pyroprocessing of used nuclear fuel (e.g., in LiCl-KCl eutectic salt)[1,2] as well as from operation of the Molten Salt Reactor Experiment (MSRE) at Oak Ridge National Laboratory (i.e., LiF-$BeF_2$ or FLiBe).[3] While these are some of the existing halide salt wastes, the proposition of Generation-IV molten salt reactors (MSRs) running in either molten chloride or fluoride salt systems could add significantly more examples to this growing list.[4-6] During pyroprocessing, used fuel is chopped up and dissolved in molten salts within an electrorefiner, the actinides are recovered through reduction at a cathode, and the fission products are released into the molten salt.[7] Several radioactive waste streams come from pyroprocessing, including the volatile fission products, the noble metal fission products that accumulate in the anode compartment alongside fuel cladding fragments, and the remaining fission products left in the molten salt.[7] The salt waste, primarily comprised of LiCl-KCl eutectic salt, is hygroscopic in air and readily soluble in water. These characteristics are highly undesirable for long-term nuclear waste storage and will likely require some type of stabilization prior to disposal.

The FLiBe-based waste from the MSRE was stored in the drain tanks until it was discovered that pressure was being generated in the tanks due to $UF_6$ production and $F_{2(g)}$ production resulting from radiolysis of the salts.[8-10] To combat these issues, the actinides were removed from the salt. Thus, it is likely that MSR salts cannot be stored in unvented containers after they exit an MSR and will require at least some post-processing to minimize gas generation once they are discharged from the reactor. An alternative approach to stabilization is to remove the halide fraction (i.e., dehalogenation) through reactions with chemical reagents to produce volatile halide byproducts that can be captured (i.e., radioactive $^{36}Cl$ with $t_{1/2}$ = $3.01\times10^5$ y or $^{129}I$ with $t_{1/2}$ = $1.57\times10^7$ y),[11,12] recycled (e.g., stable enriched $^{37}Cl$, if used for its lower neutron absorption cross section),[13] or possibly discarded (i.e., $^{19}F$).[14] Even a partial (incomplete) dehalogenation step would improve salt waste storage as well as downstream processing into waste forms, but these reactions generate secondary byproducts (e.g., HCl, HF, $NH_4Cl$).

Vitrification has been proposed as a method for disposing of such nuclear waste because once the waste is incorporated into glass, it is then present within a chemically stable matrix and protected against corrosion from the environment over geologic timescales.[15,16] However, due to the limited solubilities of halides in borosilicate glasses (i.e., the most well-studied glass waste form for nuclear waste immobilization), limited retention of halides during high-temperature vitrification, and the negative effects of dissolved halides on the long-term stability of these glasses,[17-19] effective immobilization of the salt waste produced by pyroprocessing or from MSRs within a highly loaded waste form that is chemically durable remains an ongoing topic of research for the U.S. Department of Energy.[20,21] It is likely that full dehalogenation of the salt wastes would not be required to fabricate a waste form meeting the regulatory requirements, but halides remaining in the waste prior to high-temperature processing into waste forms could volatilize during processing.

The goals of the current work were to (1) evaluate organic-acid dehalogenation agents for simple salts using a variety of acids, (2) evaluate organic-acid dehalogenation for a complex salt simulant called ERV3 (electrorefiner version 3), and (3) evaluate the properties of a borosilicate glass waste form referred to as TARS (The Average of Refined Specifications) that could be produced from an optimized formulation of glass-forming chemicals to meet glass property constraints for processing and disposal. These goals are shown graphically in Figure 1. For goal (1), the organic acids studied included oxalic acid ($H_2C_2O_4$), formic acid ($CH_2O_2$), and acetic acid ($C_2H_4O_2$) to promote the dehalogenation process at reaction temperatures ranging from 150°C to 300°C with $LaCl_3$-LiCl-KCl (7.19% 53.77% and 39.04% by mole, respectively) with 1:1, 2:1, and 3:1 molar ratios of $H^+$:$Cl^-$. Two additional acids were tested in a much more limited capacity, oxamic ($C_2H_3NO_3$) and citric acid ($C_6H_8O_7$). Experiments included modified treatments of different mass ratios of organic acid to salt simulant, different heating temperatures, and different reaction durations. For goal (2), the data acquired from (1) were used to perform the same process for the ERV3 simulant. For goal (3), glass composition-property models were utilized to formulate a borosilicate glass with high waste loading assuming full dehalogenation of the ERV3 salt simulant and conversion to oxides.

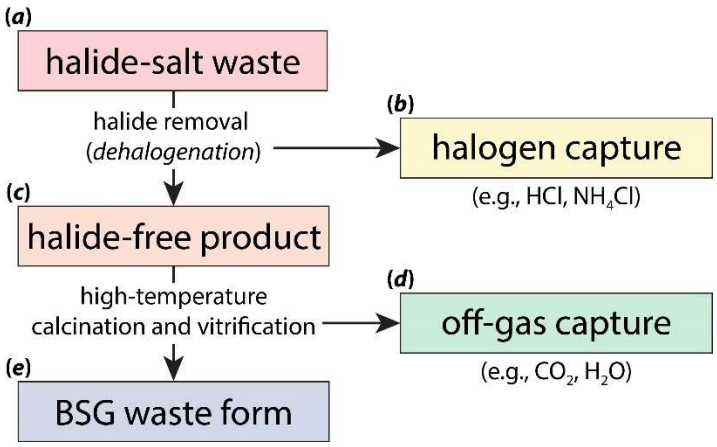


**Figure 1. Summary of study documented in this paper, including (a) the initial salt waste followed by dehalogenation (phase-1 and phase-2) and (b) halogen capture to generate (c) a halide-free product. This is then heated at a higher temperature for calcination/vitrification where (d) byproducts can be captured, and (e) the final product is vitrified into a borosilicate glass (BSG) waste form.**

## 2 Background

In recent years, work has been done on evaluating phosphate reagents [i.e., $NH_4H_2PO_4$, $(NH_4)_2HPO_4$, $H_3PO_4$] for dehalogenating halide-salt waste simulants followed by subsequent vitrification of the cations into iron phosphate waste forms.[14,22-29] The primary goal of this work was to improve salt cation loadings in resulting waste forms over the baseline technology for treating and immobilizing wastes from pyroprocessing, which is the glass-bonded sodalite ceramic waste form.[30] In 2021, a technology development roadmap[31] was produced outlining the experimental gaps in deploying the phosphate-based dehalogenation-vitrification process for treatment of radioactive salt wastes. When reacting phosphate reagents with salt waste streams, off-gas products are generated (i.e., HCl, $NH_4Cl$, $NH_4I$, $H_2O$) that differ depending on the reagent and salt composition. The salt cations are then converted to phosphates and/or oxides, and the resulting product is an alkali-rich, phosphate-based product. Since this product is not chemically durable, additional glass-forming chemicals and subsequent high-temperature vitrification steps are required to stabilize it as a waste form. One of the limitations with the phosphate dechlorination approach is that the phosphate precursors remain in the final product, so the minimum phosphate additive is determined by the dechlorination process efficiency rather than optimal waste form design. Another

limitation with some of these precursors [e.g., $NH_4H_2PO_4$, $(NH_4)_2HPO_4$] is that reacting nitrogen-based reagents with halides can generate hazardous contact explosives, e.g., $NCl_3$, $NBr_3$, $NI_3$, $NH_4I_3$.[32]

An alternative approach to using these phosphates for dechlorinating halide salt streams is to utilize a chemical reagent that decomposes, such as an organic acid, and leaves no trace in the product of the reaction where the main byproducts are HCl and $H_2O$. The general differences of organic acids and phosphate are shown graphically in Figure S1 in Supporting Information (SI). The two primary advantages of implementing fully decomposed dechlorination agents include: (1) excess reagent can be added to help maximize dechlorination efficiency without any adverse effects downstream of the process other than additional $CO_2$ production, (2) the dechlorinated waste stream can be immobilized in a variety of waste forms with high technical maturity (such as borosilicate glasses), and (3) the waste loading can be increased past what is possible with the phosphate-based processes. These points are discussed below in more detail.

Utilizing organic acids result in the conversion of chloride salts to salts of the organic acid anion (e.g., 2 KCl → $K_2C_2O_4$) through Reaction (1), which then convert to oxides (e.g., $K_2O$) through decomposition reactions [see Reaction (2)].[33] Alternatively, conversion from the organic acid anion state to an oxide could go through a carbonate transition phase (e.g., $K_2CO_3$) [see Reaction (3)].[34] Note that both decomposition reactions [i.e., Reaction (2) and Reaction (3)] generate $CO_2$, which is one of the only drawbacks to this approach as opposed to using phosphate dechlorination agents.

$$H_2C_2O_4 + 2\ KCl \rightarrow K_2C_2O_4 + 2\ HCl \quad (1)$$

$$2\ K_2C_2O_4 + O_2 \rightarrow 2\ K_2O + 4\ CO_2 \quad (2)$$

$$2\ K_2C_2O_4 + O_2 \rightarrow 2\ K_2CO_3 + 2\ CO_2 \quad (3)$$

The dehalogenation reactions between certain organic acids and halogen salts have been known since at least the early 1960s. Early investigations of this reaction, conducted by Yeh et al.[35] and Lin et al.[36] proposed a water-catalyzed reaction mechanism. Yeh et al.[35] provided a comprehensive literature overview of organic acid reactivity with halide salts as shown in Table 1. In these early studies, it was found that several acids did not react with NaCl but can react with $CaCl_2 \cdot 2H_2O$. It was also found that acids containing

moisture reacted with NaCl, but anhydrous acids yielded no reaction.[35] A relationship between decreasing pKa (i.e., acid dissociation constant) and increasing chlorine removal was also suggested in these early reports, with oxalic acid having the greatest chlorine removal potential and the lowest pKa of the acids tested.[35,36] The method of chlorine removal determination in these early studies was to use bubblers filled with a $AgNO_3$ solution, and then to gravimetrically quantify the resulting AgCl precipitate.[35,36]

**Table 1. A summary of different organic acids and their reactivities with NaCl and $CaCl_2 \cdot 2H_2O$, including acid names, alternative names (including IUPAC names), chemical formulae, melting temperature ($T_m$), density ($\rho$), the dissociation constant (pKa), and percentage of Cl removal (%$R_{Cl}$) after reactions of with NaCl or $CaCl_2 \cdot 2H_2O$ with acids and phenols. The data are sorted descending in terms of pKa. This table was modified from the original by Yeh et al.[35] and reprinted with permission. Copyright 1962 American Chemical Society.**

| Acid | IUPAC (alternative) | Formula | $T_m$ (°C) | $\rho$ (g·cm$^{-3}$) | pKa | %$R_{Cl}$ (NaCl) | %$R_{Cl}$ ($CaCl_2 \cdot 2H_2O$) |
|---|---|---|---|---|---|---|---|
| Oxalic acid dihydrate | Ethanedioic acid | $H_2C_2O_4 \cdot 2H_2O$ | 101.5 | 1.653 | 1.23 | 55.1 | 55.8 |
| Maleic Acid | (2*Z*)-But-2-enedioic acid | $C_4H_4O_4$ | 139 | 1.590 | 1.9 | 48.1 | 50.9 |
| *o*-Nitrobenzoic acid | 2-Nitrobenzoic acid | $C_7H_5NO_4$ | 147.5 | 1.575 | 2.17 | None | 48.1 |
| 3,5-Dinitrobenzoic acid | 3,5-Dinitrobenzoic acid | $C_7H_4O_6N_2$ | 205 | – | 2.80 | None | 41.8 |
| Malonic acid | Propanedioic acid | $C_3H_4O_4$ | 135[(d)] | 1.619 | 2.80 | 41.2 | 44.6 |
| Phthalic acid | Benzene-1,2-dicarboxylic acid | $C_8H_6O_4$ | 230[(d)] | 2.18 | 3.00 | 1.4 | 1.4 |
| Salicylic acid | 2-Hydroxybenzoic acid | $C_7H_6O_3$ | 159.0 | 1.443 | 3.00 | None | 44 |
| Fumaric acid | (2*E*)-But-2-enedioic acid | $C_4H_4O_4$ | 287[(d)] | 1.635 | 3.00 | None | 40.4 |
| Benzoic acid | Benzoic acid | $C_7H_6O_2$ | 122.35 | 1.2659 | 4.17 | None | 42.6 |
| Succinic acid | Butanedioic acid | $C_4H_6O_4$ | 187.9 | 1.572 | 4.19 | 38.4 | 42.6 |
| Phenylacetic acid | Phenylacetic acid | $C_8H_8O_2$ | 76.5 | 1.228 | 4.31 | None | 39.1 |
| Adipic acid | Hexanedioic acid | $C_6H_{10}O_4$ | 152.5 | 1.360 | 4.43 | 34.6 | 38.4 |
| Cinnamic acid | (2*E*)-3-Phenylprop-2-enoic acid | $C_9H_8O_2$ | 133 | 1.2475 | 4.44 | None | None |
| Palmitic acid | Hexadecanoic acid | $C_{16}H_{32}O_2$ | 62.5 | 0.8527 | 5.20 | None | 38.4 |
| Potassium biphthalate | Potassium 2-carboxybenzoate | $C_8H_5KO_4$ | – | 1.636 | 5.28 | None | 23.7 |
| Stearic acid | Octadecanoic acid | $C_{18}H_{36}O_2$ | 69.3 | 0.9408 | 5.36 | None | 9.1 |
| Phloroglucinol | Benzene-1,3,5-triol | $C_6H_6O_3$ | 218.5 | 1.46 | 7.0 | None | 0.4 |
| *p*-Nitrophenol | 4-Nitrophenol | $C_6H_5NO_3$ | 113.6 | 1.479 | 7.16 | None | None |
| *o*-Nitrophenol | 2-Nitrophenol | $C_6H_5NO_3$ | 44.8 | 1.2942 | 7.21 | None | None |
| *m*-Nitrophenol | 3-Nitrophenol | $C_6H_5NO_3$ | 96.8 | 1.2797 | 8.0 | None | None |
| Resorcinol | Benzene-1,3-diol | $C_6H_6O_2$ | 109.4 | 1.278 | 9.4 | None | None |
| Phenol | Benzenol | $C_6H_6O$ | 40.89 | 1.0545 | 10.01 | None | None |
| 2,4-Dinitrochlorobenzene | 1-Chloro-2,4-dinitrobenzene | $C_6H_3ClN_2O_4$ | 53 | 1.4982 | – | None | None |
| Phthalic anhydride | 2-Benzofuran-1,3-dione | $C_8H_4O_3$ | 130.8 | 1.527 | – | None | Trace |

[(d)] decomposes

It was not until 2022 that applying this reaction to treating salt wastes from pyroprocessing was investigated by Dong et al.,[37] who reported on the use of anhydrous oxalic acid (i.e., $C_2H_2O_4$) to dehalogenate mixed chloride salts. Chlorine removal of >90 mass% was reported at 300°C. They proposed a water-free reaction mechanism, having assumed that their reaction system was completely anhydrous. However, the system described included a series of three water bubblers attached to the heated reaction vessel, with no sweep gas or vacuum applied to ensure that the reaction vessel would not be exposed to

moist air. This work served as a basis for the current study. A description of the general flow sheet for the process described within this paper is shown schematically in Figure 2. While this flow sheet shows electrochemical salt waste as the starting point, other types of salt wastes could be included in a similar fashion, e.g., MSR wastes.

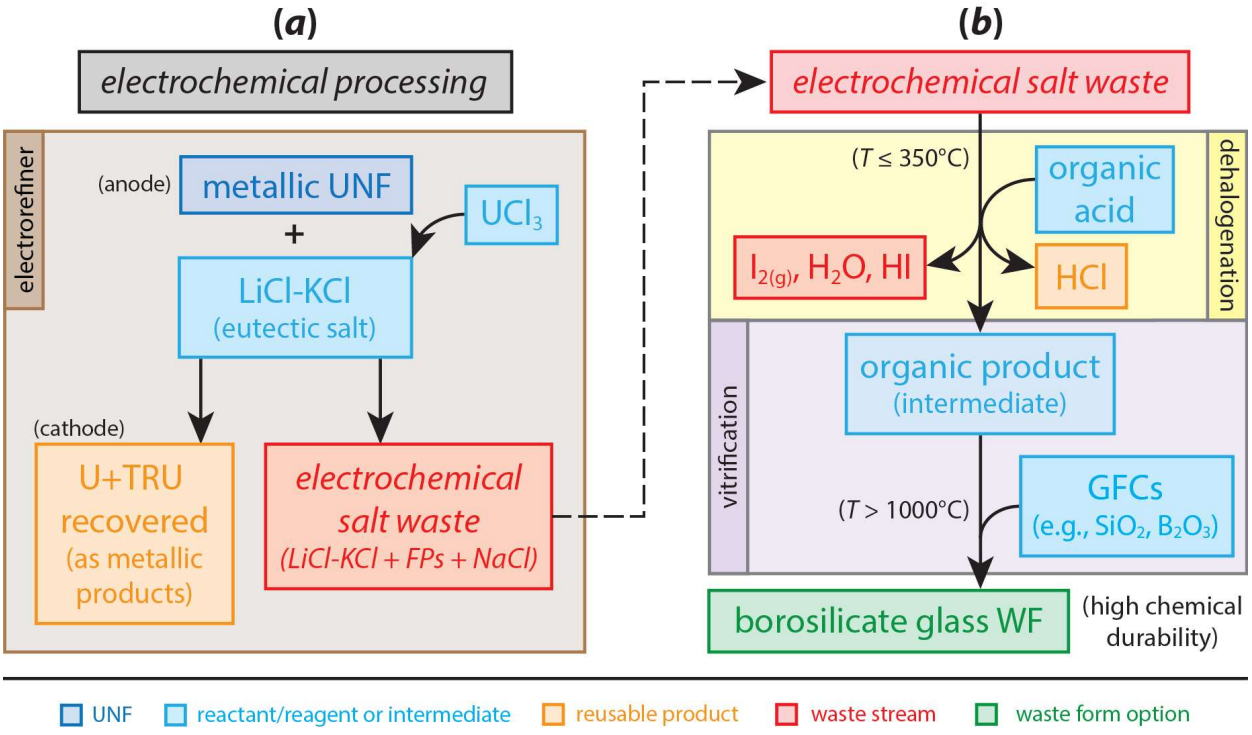


**Figure 2. Summary of (a) electrochemical processing, which generates a salt waste stream as well as (b) the general steps that can be taken to perform both dehalogenation with organic acids and vitrification of the dehalogenation products into a borosilicate glass waste form. UNF = used nuclear fuel; TRU = transuranics; FPs = fission products; GFCs = glass-forming chemicals; WF = waste form. This figure was reprinted in part with permission from Murray et al.[26] Copyright 2023 American Chemical Society.**

## 3 Experimental Methods

### *3.1 Dechlorination Experiments and Product Analysis*

Dechlorination experiments are separated by the simple salt experiments (SS, i.e., Section 3.1.1) and those run with a more complex simulant (ERV3, i.e., Section 3.1.2). A summary of the experiments discussed below is provided in Table 2. Formic acid and acetic acid were tested in addition to oxalic acid to evaluate whether the number or position of the carboxyl groups in the acid affects the dechlorination

efficiency. The target ratios were based on $H^+$:$Cl^-$ ions, so this ratio was adjusted to account for the concentration of the different starting acid solutions.

**Table 2. Summary of dechlorination experiments for both the SS and ERV3 with the $H^+$:$Cl^-$ molar ratio, the acid used, the salt, and the temperature (*T*). The "Alt. ID" entries are alternative sample identifiers used during sample preparation and are carried over to the paper and the SI so that they are not lost.**

| ID | Alt. ID | $H^+$:$Cl^-$ | Acid | Salt | *T* (°C) |
|---|---|---|---|---|---|
| SS-1 | WSU-5 | 3 | Oxalic acid | SS | 350 |
| SS-2 | WSU-6 | 3 | Oxalic acid | SS | 300 |
| SS-3 | WSU-7 | 1 | Oxalic acid | SS | 300 |
| SS-4 | WSU-8 | 3 | Oxalic acid | SS | 200 |
| SS-5 | WSU-9 | 1 | Oxalic acid | SS | 200 |
| SS-6 | WSU-10 | 3 | Oxalic acid | SS | 150 |
| SS-7 | WSU-11 | 3 | Formic acid | SS | 300 |
| SS-8 | WSU-12 | 1 | Formic acid | SS | 300 |
| SS-9 | WSU-13 | 1 | Formic acid | SS | 200 |
| SS-10 | WSU-14 | 1 | Acetic acid | SS | 300 |
| ERV3-1 | WSU-1 | 3 | Oxalic acid | ERV3 | 300 |
| ERV3-2 | WSU-2 | 3 | Oxalic acid | ERV3 | 250 |
| ERV3-3 | WSU-3 | 3 | Oxalic acid | ERV3 | 200 |
| ERV3-4 | WSU-4 | 3 | Oxalic acid | ERV3 | 150 |

### *3.1.1 Salt Dehalogenation with Simple Salt*

Initial bench studies were done thermogravimetrically without any acid vapor capture. Six small high-alumina ceramic crucibles (Coors 80104, ~20 mL capacity) were used for these experiments, divided into three groups of two (i.e., group-1: A1, A2; group-2: B1, B2; group-3: C1, C2) – see Figure S2 (SI) for a schematic and Figure S3 and Figure S4 (SI) for pictures of the experimental setup. Each crucible was weighed while empty (tare mass), and then a small amount (50–75 mg) of $LaCl_3$-LiCl-KCl salt was added to each. KCl and LiCl were sourced from Sigma-Aldrich (BioXtra, >99.0%), and $LaCl_3$ was sourced from J.T. Baker (ACS). The crucible with the salt was then placed on a ~90°C hot plate to dry before the acid was added. The mass of the crucible filled with the dry salt mass was recorded. For each experiment, a molar ratio of $H^+$ to $Cl^-$ ions was chosen of 1:1, 2:1, or 3:1, and an appropriate volume or mass of the organic acid was added to each crucible to supply these $H^+$ ions. Formic acid and acetic acid were added as 10 M

solutions, and oxalic, oxamic, and citric acid were added as dry solids. Formic acid was sourced from Sigma-Aldrich (>96% ACS), glacial acetic acid was sourced from Macron Fine Chemicals (ACS), oxalic acid dihydrate was sourced from Fisher Chemical (ACS), oxamic acid was sourced from Thermo Fisher Scientific (98%), and citric acid was sourced from Sigma-Aldrich (>99.5% ACS). Formic and acetic acid were diluted to 10 M in deionized water (DIW, i.e., 18 MΩ·cm). Chemical structures of organic acids discussed within this paper are shown in Figure 3.

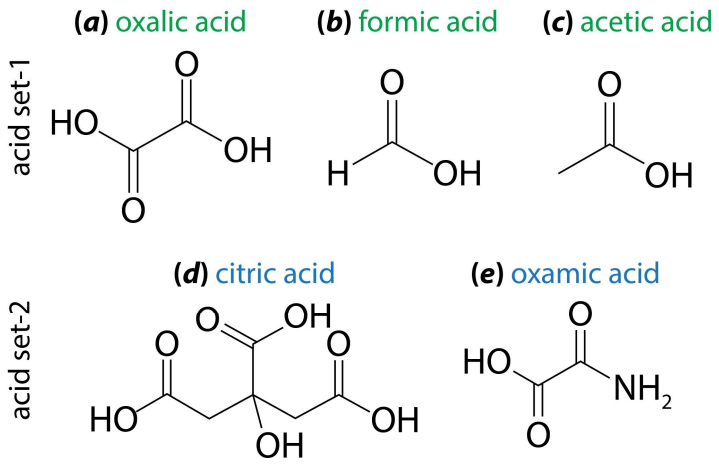


**Figure 3. Chemical structures for the five primary organic acids discussed within this paper, including (set-1, a-c) (a) oxalic acid, (b) formic acid, and (c) acetic acid as well as (set-2, d and e) (d) citric acid and (e) oxamic acid.**

The empty crucible masses and the mass of the crucibles with salt and acid were recorded before the crucibles were placed on a pre-heated hot plate set to the selected experiment temperature ($T_e$ = 150°C, 200°C, 250°C, or 300°C). The temperature of the crucibles was checked periodically using an infrared thermometer (KIZEN LaserPro LP300). Each pair of crucibles (A, B, or C) with duplicate compositions was removed from the heat at staggered 15-min intervals (i.e., crucibles A1 and A2 were removed at 5 min, crucibles B1 and B2 at 10 min, crucibles C1 and C2 at 15 min, crucibles A1 and A2 again at 20 min, and so on in a repeating cycle) so that all crucible masses could be recorded throughout the experiment. The experiment times ($t_e$) varied from 50–90 min depending on the temperature, with lower-$T_e$ experiments being longer.

At the end of the experiment, all six crucibles were weighed, the solid products were removed mechanically using a stainless-steel spatula, and the products were reserved. If the solids could not be removed easily (as was the case for the formic and acetic acid experiment products), a small amount of DIW was added to assist with removal, the dissolved product salts were collected in a glass scintillation vial, and the water was removed by heating to 90°C until only dry product salts remained.

### *3.1.2 Salt Dehalogenation with Complex Salt Simulant (ERV3)*

The ERV3 salt simulant was produced through melt-quench processing within an argon glovebox at Argonne National Laboratory. The ERV3 salt composition is provided in Table 3 with additional details documented in previous studies by Riley et al.[38-40] and Stariha et al.[41] Prior to salt dehalogenation experiments, the ERV3 salt was ground with a mortar and pestle for 10 minutes, and then dried at 90°C prior to use. Prior to grinding, the ERV3 salt pieces were blue, with some light gray surfaces. After grinding, the ERV3 powder was light blue with small gray flecks. The gray flecks are from the graphite crucible used to melt the salt.

**Table 3. Composition of the ERV3 salt simulant used in these studies.**

| Salt | Mass fraction | Mole fraction |
|---|---|---|
| KCl | 0.391 | 0.341 |
| LiCl | 0.320 | 0.493 |
| NaCl | 0.090 | 0.101 |
| CsCl | 0.070 | 0.027 |
| $CeCl_3$ | 0.050 | 0.013 |
| $NdCl_3$ | 0.049 | 0.013 |
| $SrCl_2$ | 0.030 | 0.012 |
| SUM | 1.000 | 1.000 |

Based on the results of the simple salt dehalogenation experiments (see Section 3.1), a more limited set of dehalogenation experiments were performed with the ERV3 salt. These experiments were performed with a 3:1 $H^+$:$Cl^-$ ion ratio at a temperature range of 150–300°C. To mitigate many of the problems associated with performing experiments in open crucibles, the ERV3 experiments were performed in a two-neck 250 mL round-bottom glass flask in a sand bath on a hot plate. One neck of the flask was left open,

while the other was connected to a series of three glass bubblers, and a vacuum was drawn through the bubblers to ensure that air and any vapor or gas products were pulled into the bubbler.

As in the procedure used by Yeh et al.,[35] the first bubbler was filled with a $AgNO_3$ solution. During initial bench tests, it was determined that little to no acid vapor reached the second and third bubblers (based on pH measurements of the water in the bubbler), so filling the first bubbler with 0.1M $AgNO_3$ was sufficient. The ERV3 salt was dried at 90°C prior to use, approximately 400 mg of salt was weighed out for each experiment and mixed with oxalic acid dihydrate before the powder was quickly added to the pre-heated reaction flask.

During the experiment, the vacuum pulled from the third bubbler ensured a constant airflow through the reaction flask. Gases and vapors formed during the reaction between the ERV3 salt and the organic acids in the reaction flask were drawn into the bubblers. Due to the relatively slow airflow through the reaction flask, and the lack of insulation on the top of the flask and around the tubing, significant amounts of condensation formed at the top of the flask and in the Tygon tubing between the flask and the first bubbler. Each experiment was run until there was no liquid condensate was left in the reaction flask, and after each experiment a small volume (5–10 mL) of DIW was used to rinse the connector and tubing that led from the flask to the bubbler. This was done to ensure that any remaining condensation would be pulled into the first bubbler.

White AgCl precipitate formed in the $AgNO_3$ bubbler upon contact with chlorine. After each experiment, the bubbler was emptied, the precipitate filtered out, and then rinsed several times with DIW to remove any remaining $AgNO_3$. The precipitate was then dried overnight in the dark (due to the light sensitivity of AgCl) and weighed the next day to determine the total amount of chlorine captured in the $AgNO_3$ bubbler.

During the drying and weighing of the AgCl precipitate, exposure to light could not be completely prevented. This resulted in partial decomposition of the AgCl to metallic Ag while drying, as indicated by the pale purple color of the precipitates during weighing the next day. Because the extent of decomposition

was not known, the chlorine removal calculations for each experiment were done twice following two different assumptions: one assuming that the precipitate consisted only of AgCl and the other assuming that the precipitate consisted only of Ag. It was assumed that the actual chlorine removal fraction must lay in between these two values. Additional error was introduced by a slight loss of chlorine vapor at the very start of the experiment, when the acid and salt were mixed together and placed in the hot reaction flask. Likewise, at the end of each experiment, a small volume of condensate that may contain HCl was lost in the seam between the glass connector and the neck of the flask. These losses are estimated to be quite small, but the volume of condensate lost in this way could not be quantified.

Additional experiments using 10M acetic acid were performed on ERV3 salt, but no numerical results from such experiments are reported, for reasons which will be described. No formic acid experiments were performed in this system.

### *3.1.3 Dechlorination Product Analysis*

#### 3.1.3.1 Inductively Coupled Plasma – Mass Spectrometry on Dechlorinated Products

All solutions were prepared using 18.2 MΩ·cm DIW and high-purity $HNO_3$. The 14 different dechlorinated samples (≈ 50 mg each) were provided for analysis in capped glass vials, including ten SS samples and four ERV3 samples (see Figure S10, SI). A portion of each sample (≈ 5–25 mg, averaging ≈ 15 mg) was dispensed into a cleaned plastic test tube on a balance (Model SECURA225D, Sartorius Lab Instruments, Göttingen, Germany) capable of reading to ±10 µg. The exact mass of the solid was taken before 10 mL of $HNO_3$ (2% by volume) was added, and the new mass taken. This was repeated for all 14 samples. Four of the sample powders (i.e., SS-7, SS-8, SS-9, and SS-10) completely dissolved in the dilute acid but the remaining ten appeared to be largely insoluble. The insoluble samples were those produced by reacting salts with oxalic acid, while those reacted with acetic and formic acid were readily soluble. These insoluble ten samples were placed in an ultrasonic bath for 1–2 hours to break up the solid material into finer particles that could then be easily suspended in solution on agitation. All the samples were further diluted in 2% $HNO_3$ in two 100-fold dilution steps by mass to prepare the analytical measurement solutions.

The analytical calibration solutions containing Li, Na, Cl, K, Sr, Cs, La, Ce, and Nd were all prepared by weighed serial dilution in 2% $HNO_3$ from 1000 ppm single-element standard solutions (Inorganic Ventures, Christiansburg, VA, USA). The inductively coupled plasma mass spectrometry (ICP-MS) calibration solutions were prepared at 10 ppb, 100 ppb, and 1000 ppb with Cl added in at a 10-fold higher concentration than the other elements. The ICP-MS (Model X-series, Thermo-Fisher Scientific, Winsford, UK) was operated in normal "hot plasma" mode at 1250 W. Detector cross-calibration was performed using a solution containing all the elements of interest plus In and U. The $Cl^+$ was measured at mass 35 and, while the background is elevated largely due to the presence of the molecular ion interferences, that did not hinder linear calibration at ≥ 100 ppb concentrations.

Samples were analyzed after ICP-MS calibrations with wash measurements between samples to ensure no contamination carry-over. The most diluted sample (10,000×) was run first, followed by the lower 100× dilution. The Li, Sr, Cs, La, Ce, and Nd concentration measurements were used from the 10,000× dilution, while Na, Cl, and K results were used from the lower 100× dilution as this provided the highest signal-to-background for those elements. A full mass spectrum (Li→U) was also collected and examined for the presence of any other elements at significant concentrations that might affect the results. Periodically the 10 ppb (100 ppb Cl) elemental standard was reanalyzed to ensure instrument drift would not affect the results. All elemental concentrations measured were normalized to the mass ratio (in g/g) of sample/solution, respectively, and then summed. The difference between the total analysis mass for all the measured elements and the sample mass was assumed to be made up by the elements that were not measured by ICP-MS, which include a combination of H, C, N, and O. The percent mass of each element is then given by dividing normalized measured element mass by the sample mass and multiplying by 100. Replicate sample dilutions and measurements were made on different days and a comparison between the results showed good agreement.

#### 3.1.3.2 X-Ray Diffraction

X-ray diffraction (XRD) phase identification was performed on the dechlorination solid products using a Bruker D8 Advance (Bruker AXS Inc Madison, WI) using Cu $K_\alpha$ emission and a LynxEye position-sensitive detector. Scan parameters used were a range of 5–90° 2θ with a step size of 0.015° 2θ and a 1.5-s dwell time.

## *3.2 Borosilicate Glass Formulation, Synthesis, Heat Treatment, and Testing*

### *3.2.1 Borosilicate Glass Formulation*

For the borosilicate glass formulation phase of the study, the ERV3 complex salt simulant (see Table 3) was used as a starting point. Since none of the existing glass composition-property models were developed with data containing high $Cs_2O$, $CeO_2$, and alkali concentration totals of >30 mass%, two methods (i.e., Case-1 and Case-2) were used to convert the original ERV3 salt simulant composition into something acceptable for input into the current property models. For Case-1, $Cs_2O$ was replaced by $K_2O$, and $CeO_2$ was replaced by $Nd_2O_3$ on an equal molar basis so that the property models could extrapolate. For Case-2, all the alkali oxides were converted to $Na_2O$ on an equimolar basis. A summary of these two cases is presented in Table S2 (SI). With this set of revised compositions, constraints were selected based on use of an in-can melter discussed in a previous study[42] to process the formulation into a glass melt and subsequent waste form; this removes the processability need to minimize crystallization due to the absence of a melter pour spout.[43-45] Models were utilized for these different formulations, and these are documented below in Table 4.[46-48]

**Table 4. Property and compositional constraints including melting temperature ($T_m$), viscosity ($\eta$) at $T_m$, the product consistency test response,[49] nepheline formation constraint, other crystallization constraints (i.e., from slow cooling, melt crystallization), and a multi-component model validity constraint.**

| Property | Lower limit | Upper limit | Unit | Model reference |
|---|---|---|---|---|
| $T_m$ | 1150 | 1150 | °C | (a) |
| $\eta$ at $T_m$ | 1 | 8 | Pa·s | Vienna et al.[47] |
| PCT | – | 4 | g/m$^2$ | Vienna et al.;[47] Vienna and Crum[46] |
| Nepheline | 0 | – | Distance to the line | Lu et al.[48] |
| Slow-cooled glass crystallization constraints | | | | Vienna et al.[47] |
| Melt crystallization constraints | | | | Vienna et al.[47] |
| Multi-component model validity constraint $w_{Na_2O} + 0.66w_{K_2O} + 2.07w_{Li_2O} < 27.018$ mass% | | | | Vienna et al.[47] |

Glasses were formulated by maximizing waste loading and varying the amount of glass-forming chemicals (GFCs) so that the final glass satisfies all the property constraints (or as many as possible). Then, final glass compositions were calculated based on waste and GFC loadings, as shown in Table 5. From these calculations, the predicted properties for Case-1 and Case-2 are presented in Table S3 (SI). The glass that was produced for characterization was a formulation that fell in the middle of Case-1 and Case-2 (i.e., an average), which was called TARS (The Average of Refined Specifications).

**Table 5. Glass compositions for Case-1 and Case-2 with waste loadings shown at the bottom in terms of total oxide mass and total salt cation mass. TARS is an average of both cases and is the glass that was made for this study.**

| Category | Modeling | | | Experimental | | | |
|---|---|---|---|---|---|---|---|
| | Oxides | Case-1 (mass%) | Case-2 (mass%) | Oxides | TARS (mass%) | Additive | Mass (g) |
| GFCs | $Al_2O_3$ | 8.000 | 8.360 | $Al_2O_3$ | 8.180 | $Al_2O_3$ | 40.900 |
| | $B_2O_3$ | 9.000 | 9.320 | $B_2O_3$ | 9.160 | $H_3BO_3$ | 81.354 |
| | CaO | 8.000 | 6.810 | CaO | 7.410 | $CaCO_3$ | 66.127 |
| | $SiO_2$ | 37.480 | 37.900 | $SiO_2$ | 37.680 | $SiO_2$ | 188.400 |
| | ZnO | 3.500 | 2.000 | ZnO | 2.750 | ZnO | 13.750 |
| | $ZrO_2$ | 4.000 | 4.000 | $ZrO_2$ | 4.000 | $ZrO_2$ | 20.000 |
| Waste | $CeO_2$ | 1.900 | 2.000 | $CeO_2$ | 1.950 | $CeO_2$ | 9.750 |
| | $Cs_2O$ | 3.180 | 3.350 | $Cs_2O$ | 3.270 | $Cs_2CO_3$ | 18.903 |
| | $K_2O$ | 13.390 | 14.090 | $K_2O$ | 13.740 | $K_2CO_3$ | 100.797 |
| | $Li_2O$ | 6.130 | 6.450 | $Li_2O$ | 6.290 | $Li_2CO_3$ | 77.770 |
| | $Na_2O$ | 2.590 | 2.730 | $Na_2O$ | 2.660 | $Na_2CO_3$ | 22.744 |
| | $Nd_2O_3$ | 1.770 | 1.870 | $Nd_2O_3$ | 1.820 | $Nd_2O_3$ | 9.100 |
| | SrO | 1.060 | 1.120 | SrO | 1.090 | SrO | 5.450 |
| WL | Oxides | 30.020 | 31.610 | Oxides | 30.820 | – | – |
| | Cations | 22.845 | 24.057 | Cations | 23.456 | – | – |

GFC = glass-forming chemical; WL = waste loading

### *3.2.2 Glass Fabrication*

Initial scoping studies of the ERV3-TARS formulation suggested that melting the glass at 1050°C was insufficient to melt the high amount of $CeO_2$ in the glass. The glass (targeting 500 g of final glass) was batched from reagent-grade chemicals, homogenized within an agate milling chamber, loaded in a Pt/10%Rh crucible to melt at 1150°C (± 10°C) for 1 hour with a lid within a high-temperature furnace (Deltech Inc., Denver, CO), and then the melt was poured onto an Inconel quench plate. Once cooled, the glass was milled in a tungsten carbide milling chamber to homogenize and size reduce and then it was melted for a second time under the same conditions as before and quenched. The final quenched product is referred to as ERV3-TARS-Q, which ended up containing a small amount of undissolved $CeO_2$.

### *3.2.3 Canister Centerline Cooling Heat Treatment*

Approximately 200 g of ERV3-TARS-Q glass was treated in a Pt/10%Rh crucible to create a canister centerline cooling (CCC) specimen to simulate a slow-cooling curve of a Hanford high-level waste canister. The glass was placed in a bottom-load Deltech furnace and was first held at $T_p$ for 30 min before

being treated at preset temperature setpoints and hold times to simulate the centerline cooling curve for a Hanford high-level waste (HLW) glass canister used at the Hanford Waste Treatment and Immobilization Plant.[50] The material resulting from this heat treatment was called ERV3-TARS-CCC, which was subjected to some additional characterizations described below. The thermal profile used for this heat treatment is provided in Figure S5 (SI).

### *3.2.4 Chemical Durability Testing*

Static chemical durability assessments for both the ERV3-TARS-Q and ERV3-TARS-CCC glasses were performed via both the 28-day MCC-1 test (ASTM C1220)[51] and the 7-day PCT-A test (ASTM C1285).[49] Both procedures were performed in ASTM type-1 ultrapure DIW (>18.0 MΩ·cm)[52] at a temperature of 90±2°C. The MCC-1 testing was performed via a slight deviation from ASTM C1220-21,[51] in which additional static samplings were taken at the timepoints of 7 days and 14 days, rather than the typical single timepoint of 28 days. The chosen specimens were rectangular coupons cut from the glass section and polished to a finish of 600 grit. The test was conducted with a $SA/V$ (surface area to volume) ratio of 10 $m^{-1}$ in a 60 mL Savillex PFA vessel and specimen basket.

The PCT-A test was performed in accordance with ASTM C1285-21.[49] Glasses were fractioned out with a particle size between 75 – 150 μm and were added to Type 304L stainless steel vessels with ratios of 1.5 g of solids to 15 mL of the test medium. Aliquots of both static tests were filtered and acidified with 0.1 mL of concentrated $HNO_3$. Chemical analysis of the glass leachate was performed via inductively coupled plasma optical emission spectroscopy (ICP-OES) and mass spectroscopy (ICP-MS). Normalized loss of the element (i) of interest ($NL_i$) was calculated by means of Equation (4).[49] Here, $c_i$ refers to the concentration of the element of interest ($g \cdot L^{-1}$), $V$ is the volume of DIW added (L), $SA$ is the surface area glass specimen ($m^2$), and $f_i$ is the mass fraction of the element ($g\ g^{-1}$). The $SA$ for the PCT powder was determined by Equation (5), where $m$ is the mass of the glass solids (g), $\rho$ is the measured density of the glass ($g \cdot cm^{-3}$), and $d$ is the assumed average diameter of the glass particles (cm). It should be noted that $d$ values were

based on the average of the upper and lower sieve side, volume of DIW added was assumed 1 g ≈ 1 mL, and dilution factor related to the 0.1 mL of added $HNO_3$ was considered negligible.

$$NL_i = \frac{c_i * V}{SA * fi} \quad (4)$$

$$SA = \frac{6m}{\rho d} \quad (5)$$

### *3.2.5 Glass and Melt Characterization*

Pictures of the TARS samples were taken with a digital camera with rulers in the fields of view. Optical microscopy (OM) of the glass specimens was performed with a Keyence VHX-7000 system. Scanning electron microscopy (SEM) was performed with a JSM-7001F field-emission gun microscope (JEOL USA, Inc.; Peabody, MA). Energy dispersive X-ray spectroscopy (EDS) was performed using an Oxford Instruments Ultim Max equipped with a 100 $mm^2$ window and analyzed using AZtec software. Samples were mounted in epoxy and cross-section polished to a 3-µm finish for SEM/EDS analysis. Viscosity was determined using the rotating spindle method[53] with a Brookfield LVTD viscosity head (AMETEK Brookfield, Middleboro, MA) and a Pt spindle head. Glass bulk density was calculated using an AccuPyc II 1340 He gas pycnometer for volumetric measurements and an analytical balance for mass measurements (± 0.1 mg).

Isothermal treated samples for liquidus temperature ($T_L$) determination via ASTM C1720-21[54] with the crystal fraction method were loaded into a Deltech bottom load furnace in 1.2 $cm^3$ Pt/10%Rh foil boats. Samples were melted at $T_p$ (1150°C ± 5°C) for 30 min before being directly transferred hot into the treatment furnace. The samples soaked for 24 ± 2 hours at treatment temperatures above 900°C, or for longer periods of time for below 900°C.

XRD phase identification was performed by using a Bruker D8 Advance (Bruker AXS Inc Madison, WI) using Cu $K_\alpha$ emission and a LynxEye position-sensitive detector. Semi-quantitative analysis was performed by spiking glass powder specimens with 5 mass% $TiO_2$ (NIST SRM-674b).[55] Scan

parameters used were a range of 5–90° 2θ with a step size of 0.015° 2θ and a 1.5-s dwell time. Differential scanning calorimetry (DSC) was collected on ERV3-TARS-Q glass powder using a Netzsch Simultaneous DSC-Thermogravimetric Analyzer (STA449 F1 Jupiter) equipped with an automatic sample carrier. Argon as used as both a purge and protective gas at a constant flow rate of 20 mL $min^{-1}$. The sample was heated from room temperature to 1150°C at a heating rate of 10 K $min^{-1}$ in a Pt crucible. The onset of glass transition temperature, $T_g$, was determined from the DSC data.

Data processing and plotting were conducted with Microsoft Excel (Office 365), OriginPro (2021b), and Igor Pro (v8.0.4.2, build 34722). Image collages were created with Adobe Photoshop (v26.3.0).

## 4 Results

### *4.1 Salt Dehalogenation Experiments*

#### *4.1.1 Dehalogenation Experiments with Simple Salts*

The mass loss exhibited by salt-acid mixtures primarily consists of three contributions, including (1) release of the crystalline and/or surface-adsorbed water from the salts and in the concentrated acids; (2) release of chloride from $LaCl_3$-LiCl-KCl as gaseous HCl; and (3) the vaporization of acids during boiling (at certain high temperatures). However, due to the cooccurring mass loss of water and acid during dechlorination reactions, changes in mass% values for the mixtures are not well-suited indicators for the examination of halogen removal. The masses lost from the reaction vessels during heating to 150–300°C always exceeded the combined mass of water present in the acid and salt, and the expected mass of HCl generated by the salt. The additional mass losses, which cannot be explained by water or HCl, is presumed to be loss of acid due to boiling (and splattering) as the boiling of formic acid was quite vigorous across the entire temperature range tested, and even the oxalic acid boiled at 250–300°C. This is supported by experiments in which the acids were heated without any salts presents, and the mass loss in the acetic and formic acid experiments at 150–300°C matched the mass of acid and water added to the vessel.

To address this concern, efficacies of dehalogenation were calculated by making the following assumptions: (1) a majority of the $H_2O$ is removed along with chloride during the first 5 min of the reactions; (2) the only water present in the reactions is that from the reagents; and (3) vaporization of the acids during heating contributes to mass loss and must be considered in these calculations. Using these assumptions, the total water content in the system may be estimated and corrected for yielding the approximate halogen removal efficacy. These assumptions allowed for calculating the halogen removal efficacy for all temperatures tested using a combination of known water masses, experimental data on acid vaporization during heating, and known chlorine content of the salts.

The acetic acid, formic acid, and oxalic acid all exhibited high apparent chlorine removal efficiencies (75–100%) in the thermogravimetric experiments. However, data reported in Section 4.1.2 indicate that despite these assumptions and corrections, the estimated removal efficiencies of acetic and formic acid are likely overestimated due to unaccounted sample loss during boiling. Since no silver titration experiments were performed for formic acid or acetic acid, it is unclear whether they achieved significant dechlorination, or if the apparent chlorine removal was solely due to particulate ejection during boiling. In contrast, oxalic acid-based dechlorination yielded more reliable chlorine removal efficiency values, as its solid-solid reaction mitigates issues related to acid boiling and evaporation. Specifically, the chlorine removal efficiencies increase with increasing temperature and decrease with increasing $H^+$:$Cl^-$ ion ratios (although the ion ratio only accounted for a <5 mass% difference in chlorine removal in most experiments). These results are largely consistent with the silver titration experiments in Section 4.1.2, though the thermogravimetric experiments yielded higher chlorine removal efficiencies at 250–300°C than the silver titration experiments. It is unclear whether this discrepancy arises from a slight positive bias in the thermogravimetric experiments at high temperatures when oxalic acid begins to vaporize, or a slight negative bias in the silver titration experiments due to incomplete condensate capture in the $AgNO_3$ bubbler. All the supporting data from these experiments are presented in Table S4, Table S5, and Figure S6 – Figure S9 (SI). The results from these SS studies showed that oxalic acid was the most promising acid for effective

dechlorination, and that the higher $H^+$:$Cl^-$ molar ratio was preferred (i.e., $H^+$:$Cl^-$ = 3). Therefore, the ERV3 experiments utilized these with a temperature range of 150–300°C, which are discussed in the next section.

### *4.1.2 Dehalogenation Experiments with ERV3 Salt*

The results of using oxalic acid on ERV3 are shown in Figure 4, with upper and lower bounds for the chlorine removal efficiencies. The upper bound of chlorine removal shown in Figure 4 assumes complete AgCl decomposition following the modified Mohr titration procedure, while the lower bound assumes no decomposition. The light purple coloration of the precipitates may be indicative of partial AgCl decomposition; however, the exceptionally high removal efficiencies (>100%) at the upper boundary likely result from overestimation under the assumption of full AgCl decomposition. Therefore, the chlorine removal efficiencies derived from the modified Mohr titration should be considered broad estimates. The chlorine removal as quantified by the modified Mohr titration procedure shows a decreasing trend with increasing temperature, in contrast to the results of the thermogravimetric experiments (see Figure S22, SI), which showed an increasing chlorine removal with increasing temperature. The decrease in efficiencies may be attributed to the positive bias caused by the loss of small salt particulates due to acid volatilization at high temperatures, where the melting point of oxalic acid (190°C) plays a crucial role. At $T \approx 150$°C, oxalic acid and ERV3 salt undergo a solid-solid reaction. At $T > 200$°C, the acid-salt mixture partially melted and possibly vaporized, with increasing intensity at higher temperatures. Additionally, as oxalic acid melts, its higher vapor pressure accelerates acid loss through vaporization, as evidenced by the needle-like crystals forming along the upper walls of the reaction flask during the 200–300°C experiments (Figure S6, SI). The extent of crystal formation increased with temperature, suggesting greater oxalic acid loss at higher temperatures. In contrast, minimal crystal formation was observed at 150°C and, when present, the crystals formed near the bottom of the reaction vessel instead of near the top, likely due to reduced volatilization at lower temperatures.

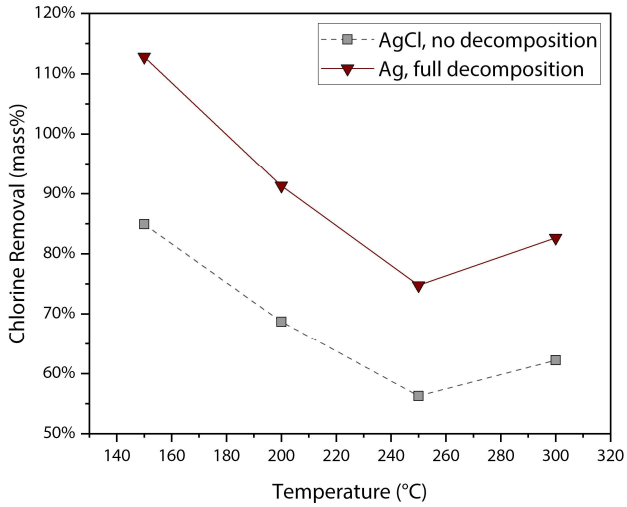


**Figure 4. Chlorine removal from the reaction of ERV3 with oxalic acid, with a 3:1 ratio of $H^+$ to $Cl^-$ ions, as indicated by the formation of AgCl precipitates within a $AgNO_3$ bubbler.**

Attempts to replicate the method of chlorine removal determination using $AgNO_3$ solution from Yeh et al.[35] within this work revealed that this method may have resulted in an underestimation of chlorine removal, as it is not reported whether multiple $AgNO_3$ bubblers were utilized or whether the AgCl was exposed to light prior to weighing. Thus, the reported chlorine removal efficiencies are lower than reported in subsequent studies described below and in the current work. Overall, the range of chlorine removal% determined by silver precipitation completely overlaps with the range observed in the oxalic acid thermogravimetric experiments, though the precise trends across the 150–300°C temperature range are not in agreement between those two methods. In addition, the use of acetic acid on ERV3 yielded no precipitates from the thermogravimetric experiments, likely due to the violent boiling of acetic acid at high temperatures. During acetic acid experiments using the $AgNO_3$ bubbler procedure, white salts were found on the upper walls of the reaction flask, not from vapor crystallization, but from intense boiling ejecting small particles. This observation suggests that the removal efficiencies of acetic acid and formic acid on simple salts (Table S4 and Table S5, SI) may have been overestimated partially due to particulate ejection from the open crucibles rather than actual dechlorination.

### *4.1.3 Analysis of Dechlorinated Samples*

With the ICP-MS data provided in Table S6 (SI), several subsequent calculations were made to study the information. First, the mass ratio ($m_r$) of target elements from the starting salt simulants (targeted compositions) were compared to the measured mass ratios of each set of elements as shown in Equation (6) where $m_{X1}$ and $m_{X2}$ denote the two elements of interest. For these calculations, everything was ratioed to Li and these values are presented in Figure S11 (SI). Additionally, since the salt compositions could vary from the target compositions for different reasons, the amount of Cl present in the starting salt was calculated based on the batched salt additives using the cation masses measured with ICP-MS and back-calculating the starting salt masses from those values. Equation (7) and Equation (8) were used to make these assessments, where $Cl_{rem.}$ and $Cl_{total}$ denote the Cl removed and the total Cl present in the starting salt, respectively. For Equation (8), $m_i$ and $m_{Cl}$ are the measured mass of element "i" and Cl from ICP-MS, respectively, $X_{Cl}$ is the number of moles of Cl in each salt (e.g., $X_{Cl}$ for $NdCl_3$ = 3), $MW_{Cl}$ is the molecular weight of Cl, and $MW_i$ is the molecular weight of cation "i" of interest. All Cl contributions from each salt associated with each cation from each simulant were combined. The calculated data are provided in Table S7 (SI).

$$m_r = \frac{m_{X1}}{m_{X2}} \tag{6}$$

$$\%efficiency = \frac{Cl_{rem.}}{Cl_{total}} \cdot 100 \tag{7}$$

$$efficiency = \frac{\left(\sum_{i=1}^{n} \frac{m_i \cdot X_{Cl} \cdot MW_{Cl}}{MW_i} - m_{Cl}\right)}{\sum_{i=1}^{n} \frac{m_i \cdot X_{Cl} \cdot MW_{Cl}}{MW_i}} \tag{8}$$

**Table 6. Summary of parameters for dechlorination experiments run with ERV3 and SS salt simulants.**

| ID | $H^+$:$Cl^-$ | Acid | Salt | *T* (°C) | $\%Cl_{resid.}$ (mass%) | $\%Cl_{rem.}$ (mass%) |
|---|---|---|---|---|---|---|
| SS-1 | 3 | oxalic acid | SS | 350 | 1.7 | 98.3 |
| SS-2 | 3 | oxalic acid | SS | 300 | 6.1 | 93.9 |
| SS-3 | 1 | oxalic acid | SS | 300 | 14.2 | 85.8 |
| SS-4 | 3 | oxalic acid | SS | 200 | 10.0 | 90.0 |
| SS-5 | 1 | oxalic acid | SS | 200 | 10.6 | 89.4 |
| SS-6 | 3 | oxalic acid | SS | 150 | 12.6 | 87.4 |
| SS-7 | 3 | formic acid | SS | 300 | 35.9 | 64.1 |
| SS-8 | 1 | formic acid | SS | 300 | 35.7 | 64.3 |
| SS-9 | 1 | formic acid | SS | 200 | 48.4 | 51.6 |
| SS-10 | 1 | acetic acid | SS | 300 | 50.0 | 50.0 |
| ERV3-1 | 3 | oxalic acid | ERV3 | 300 | 5.3 | 94.7 |
| ERV3-2 | 3 | oxalic acid | ERV3 | 250 | 8.4 | 91.6 |
| ERV3-3 | 3 | oxalic acid | ERV3 | 200 | 1.2 | 98.8 |
| ERV3-4 | 3 | oxalic acid | ERV3 | 150 | 0.2 | 99.8 |

These calculations can be caveated by the following: (1) they assume that all precipitates were dissolved through the acid and so analyzed concentrations are representative of the actual compositions; (2) while small masses of salts were used for ICP-MS, it is assumed that these aliquots were representative of the entire sample; and (3) the ICP-MS cannot be used to quantify several elements (i.e., H, C, N, O), most of which were likely or definitely present in these samples. However, these values are a good estimation of the Cl content remaining in the products.

XRD analysis of the dechlorinated salts indicates that residual amounts of chlorine in the form of sylvite (KCl) may be present in the sample post-dechlorination, which are presented in Figure S12–Figure S19 (SI), which is contrary to the ICP-MS results. However, it is important to note that the XRD results for the salts were less quantifiable due to the difficulty of fitting the peaks and the possible presence of organic species in some samples. While the Rietveld refinements of XRD data provide a breakdown of the crystalline phase distributions, it is possible that portions of these salts were amorphous and nondiffracting.

### *4.2 TARS Glass Property Measurements*

The ERV3-TARS-Q glass appeared amorphous and was pink to light purple in color (Figure 5a), but the color changes in different lighting environments due to the Nd content. The ERV3-TARS-CCC glass was visually opaque due to the increased crystallinity and a similar color to the ERV3-TARS-Q glass albeit with a more purple and less pink appearance (Figure 5b). Based on the DSC curve, the glass transition temperature ($T_g$) of the ERV3-TARS-Q glass was estimated to be 446.2°C, which is shown in Figure S22 (SI). Measured density of the quenched glass by the He pycnometer method was 2.721 g·cm$^{-3}$. The viscosity values measured at various temperatures are listed in Table S10 (SI) with fitted data presented in Table S11 (SI) and Figure S23 (SI).

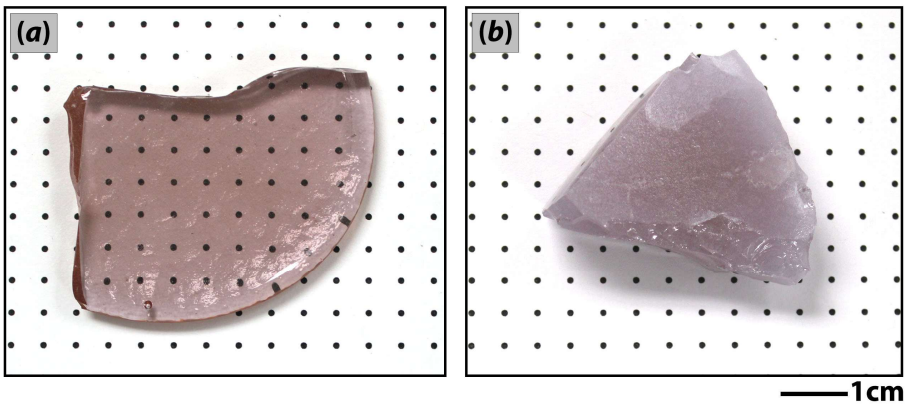


**Figure 5. Pictures of (a) ERV3-TARS-Q after two melts at 1150°C for 1 hour and (b) ERV3-TARS-CCC. The images were taken on a peg-board background so that the sample transparency could be visualized.**

The normalized loss ($NL_i$) values for B, Na, and Si (i.e., $NL_B$, $NL_{Na}$, $NL_{Si}$ in g·m$^{-2}$, respectively) for both PCT and MCC-1 testing are listed in Table 7 (more details are provided in Table S7 and Table S9, SI). Here "±" refers to standard deviations of ±1$\sigma$. Additional chemical durability data are presented in Figure S21 (SI).

**Table 7. Measured normalized loss values ($NL_i$, g·m$^{-2}$) of boron ($NL_B$), sodium ($NL_{Na}$), and silicon ($NL_{Si}$) for both the PCT test (ASTM C1285-21) and MCC-1 test (ASTM C1220-21).**

| Test | Glass ID | Interval (Days) | $NL_B$ (g·m$^{-2}$) | $NL_{Na}$ (g·m$^{-2}$) | $NL_{Si}$ (g·m$^{-2}$) |
|---|---|---|---|---|---|
| PCT-A | ERV3-TARS-Q | 7 | 0.39 ± 0.01 | 0.85 ± 0.02 | 0.20 ± 0.01 |
| | ERV3-TARS-CCC | 7 | 0.22 ± 0.00 | 0.52 ± 0.01 | 0.17 ± 0.00 |
| MCC-1 | ERV3-TARS-Q | 28 | 10.32 | 11.43 | 8.18 |
| | ERV3-TARS-CCC | 28 | 10.24 | 11.28 | 8.19 |

The XRD patterns from the quenched TARS sample and $T_L$ specimens are provided in Figure S24–Figure S31 (SI). Semiquantitative XRD analysis results indicate that the primary crystalline phase found in the heat-treated samples is either $CeO_2$ or a binary cubic zirconia structure stabilized with ceria in the form of $Ce_{0.8}Zr_{0.2}O_2$.[56] Due to the peak overlaps between $CeO_2$ and $Ce_{0.8}Zr_{0.2}O_2$ as well as the smaller quantity of $CeO_2$ in the isothermally heat-treated samples, it was difficult to distinguish between the two phases with XRD. However, OM and EDS analysis revealed trace $CeO_2$ in the isothermally heat-treated samples. The $T_L$ predicted using the crystal fraction method from ASTM C1720-21[54] for the cubic zirconia phase was determined to be 1154°C (Figure 6), which is just above processing temperature of the glass (1150°C). Other significant phases include zircon ($ZrSiO_4$), which appear in the CCC specimen and around idling temperature (950°C) and below. Analysis of low-temperature (below 900°C) isothermally heat-treated samples and CCC samples also show possible additional K-rich crystalline phases, including a K-zirconosilicate phase and a K-aluminosilicate phase. Further evidence of these phases forming can be seen in the TGA data (Figure S22, SI), where there appeared to be an exothermic peak in between $T_g$ and 900°C. A summary of possible crystalline phases for the measured crystal fraction samples is compiled in Table 8. A complete summary of crystalline phases including the CCC treated glass and lower temperature samples (< 900°C) can be found in Table S12 (SI).

**Table 8. XRD summary (mass%) of possible crystalline phases of ERV3-TARS glass at different temperature conditions. Here $R_{wp}$ refers to the weighted profile residual of the Rietveld refinement (goodness of fit assessment) and "CF" refers to the isothermal treated samples for crystal fraction.**

| Formula | ICSD# | System | Space Group (#) | Quench | 950°C-CF | 1000°C -CF | 1050°C -CF | 1100°C -CF | 1150°C -CF |
|---|---|---|---|---|---|---|---|---|---|
| $CeO_2$ | 262755 | Cubic | *Fm*-3*m* (225) | -* | -* | -* | -* | - | - |
| $Ce_{0.8}Zr_{0.2}O_2$ | 258060 | Cubic | *Fm*-3*m* (225) | – | 1.018 | 0.762 | 0.551 | 0.258 | -* |
| $ZrSiO_4$ | 95249 | Tetragonal | *I*41/*amdZ* (141) | – | 2.336 | – | – | – | – |
| $R_{wp}$ | – | – | – | – | 5.119 | 4.115 | 3.958 | 3.886 | 3.732 |

*Not detected with XRD, however SEM/EDS suggests that a small quantity may be present.

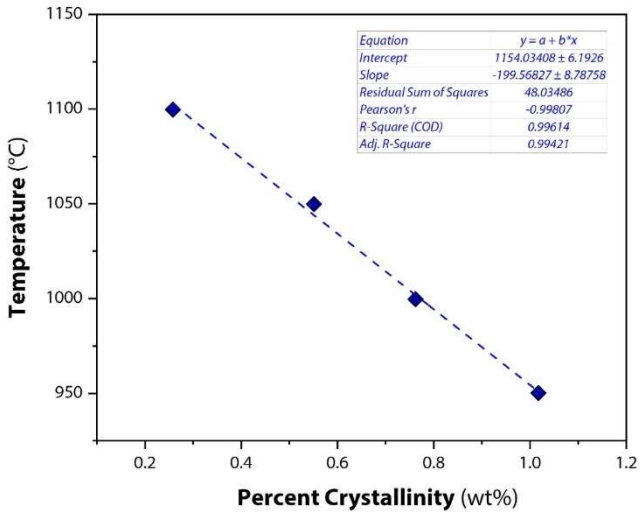


**Figure 6. Extrapolated heat-treatment temperature vs crystal fraction data (inverse plot) of the $Ce_{0.8}Zr_{0.2}O_2$ phase. The *y*-intercept is determined as the $T_L$ value (i.e., 1154°C).**

Optical micrographs of the glass samples are provided in Figure 7a,b and Figure S20 (SI). From Figure S20a (SI), the quenched material did contain some undissolved $CeO_2$, which was verified by EDS and XRD analyses (described above). Figure 7b shows the different appearances of the inclusions found in the heat-treated sample ERV3-TARS-950°C. From Figure S20b (SI), the CCC sample showed a large volume fraction of crystallization. The isothermally heat-treated samples produced from $T_L$ measurement determinations are shown in Figure 7, Figure S20c (SI), and Figure S20d (SI).

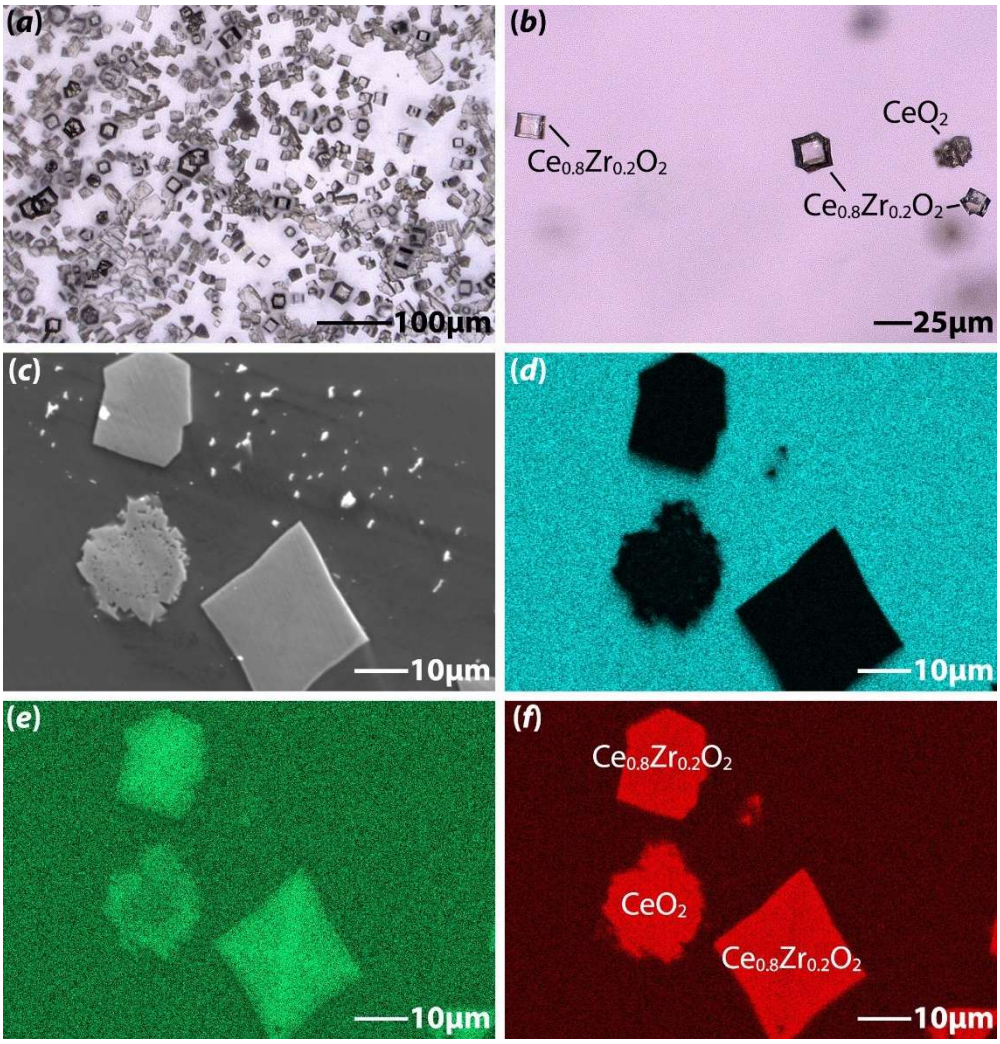


**Figure 7. (a, b) Optical micrographs, (c) scanning electron micrograph, and (d-f) energy dispersive X-ray spectroscopy elemental dot maps for the ERV3-TARS-950°C crystal fraction specimen, including (d) Si, (e) Zr, and (f) Ce. For (a) and (b), the images are seen in both transmitted and reflected light at different locations and magnifications.**

## 5 Discussion

### *5.1 Salt Dehalogenation*

Both the thermogravimetric and silver titration results for oxalic acid indicate significant dehalogenation of both the simple chloride salt and ERV3 salt mixtures. The results from acetic acid and formic acid were deemed unreliable. The measured chlorine removal efficiency was initially hypothesized to increase with decreasing pKa of the tested acids, as suggested by existing literature on organic acid and

chloride salt reactions.[35,36] Recognizing the differences between solid-solid reactions (as in the case of oxalic acid across much of the temperature range tested) and solid-aqueous reactions (as observed with formic and acetic acid), we can still examine the impact of acid pKa on dechlorination. Given its low pKa of 1.25, oxalic acid would be expected to be significantly more reactive than formic and acetic acid. However, while the $pKa_1$ of oxalic acid is lower than both formic and acetic acid (Table S1, SI), its $pKa_2$ falls between the pKa values of formic acid and acetic acid. If the dechlorination rate were limited by the second dissociation step ($pKa_2$), then oxalic acid would be expected to yield chlorine removal efficiencies between those of formic acid and acetic acid.

Additionally, the pKa values reported in Table S1 (SI) for each acid in water from the current study may not be entirely accurate or applicable for this reaction. In particular, there are literature data indicating that the pKa of carboxylic acids in chloride salt solutions is dependent on the salt concentration, and there is very little information on reaction kinetics in molten oxalic acid (as was the case in many of the oxalic acid experiments). It has been reported that the pKa values of both formic and acetic acid increase in low-concentration chloride salt solutions (as compared to literature pKa values for acids in water), and that pKa values then decrease at high salt concentrations.[58,59] The salt concentration in the formic and acetic acid experiments would have increased significantly as the excess water present vaporized, so it may not be correct to assume that the pKa of the acids is constant or matches the literature values during these experiments.

Furthermore, while the preliminary thermogravimetric results appeared to support such correlation (see Table S4, SI), subsequent dechlorination testing on ERV3 with its removal efficiency examined by the silver titration raised doubt about the accuracy of the initial thermogravimetric results for acetic acid and formic acid. Since no successful silver titration experiments were performed with these two acids, it remains unclear whether acetic or formic acid genuinely facilitated simple salt dehalogenation, or whether the appearance of chlorine removal was an artifact mass loss due to ejection of particles during boiling.

Therefore, based on this preliminary work, we cannot reliably establish a correlation between the pKa of an acid and its salt dechlorination efficiency, leaving this as a possible hypothesis for further investigation.

### *5.1.1 Proposed Reactions*

There are currently two proposed mechanisms for the dechlorination of chloride salts by organic acids. Dong et al.[37] proposed an anhydrous reaction in which oxalic acid (or other organic acids, presumably) reacts directly with chlorine salts. The proposed reaction from Dong et al.[37] is shown in Reaction (9) [i.e. a general version of Reaction (1) discussed previously]. Earlier papers by Yeh et al.[35] and Lin et al.[36] proposed a reaction in which water is involved, but not consumed. These papers did not propose an explicit model for the reaction of oxalic acid and chloride salts. Instead, they proposed a general model for these types of reactions in which a hydrogen is removed from the acid to produce a hydronium ion ($H_3O^+$), which reacts with the chloride salt to form hydrochloric acid and water.[35,36] Based on the generalized mechanism proposed by Yeh et al.,[35] an oxalic acid reaction based on that work is presented below in Reaction (10) and Reaction (11). The moisture for these reactions could be supplied by the water molecules presented in oxalic acid dihydrate (the form which was used in the experiments reported herein). Presumably, whichever reaction is true for oxalic acid, it will be similar to the reactions that occur between chloride salts and other organic acids.

$$H_2C_2O_4 + 2\ ACl \rightarrow A_2C_2O_4 + 2\ HCl \quad (9)$$

Step 1: $$H_2C_2O_4 + 2\ H_2O \rightarrow C_2O_4^{2-} + 2\ H_3O^+ \quad (10)$$

Step 2: $$C_2O_4^{2-} + 2\ H_3O^+ + 2\ ACl \rightarrow A_2C_2O_4 + 2\ HCl + 2\ H_2O \quad (11)$$

It is not entirely clear which proposed mechanism is correct, but the experiments reported here confirmed that this dechlorination reaction can occur in the presence of water. The chlorine removal achieved using oxalic acid dihydrate in a 1:1 $H^+$:$Cl^-$ molar ratio was approximately 80% at 150°C, 90% at 200°C, and up to 100% at 300°C. Dong et al.[37] report 80% chlorine removal at 200°C, and 95–100% at 300°C using anhydrous oxalic acid. Clearly the presence of water has no negative effect on this reaction,

and the more expensive anhydrous oxalic acid can be substituted for the significantly cheaper oxalic acid dihydrate if so desired.

Confirming whether the oxalic acid and chloride salt reaction can proceed anhydrously would be necessary to prove whether the proposed anhydrous or water-catalyzed reaction is correct. Unfortunately, this reaction would be very difficult to perform in a completely water-free system. Not only would the reactants need to be completely dry, but the reactions would have to be kept from absorbing water present in the air, such as from bubblers or ambient humidity (i.e., it would be best done in a moisture-free glovebox or hot cell). Despite the claims of Dong et al.[37] to have used this reaction in a water-free environment, the experimental design illustrated in that publication shows the reaction flask connected directly to a water bubbler without any sweep gas or vacuum pulled to prevent the moist air from moving from the bubbler to the reaction vessel. Thus, it is assumed that some water vapor could have been present within the reaction vessel. For this reason, further confirmation is needed for understanding the reaction mechanism to determine whether this reaction can proceed without water. Likewise, the potential involvement of acid reduction or decomposition products in the dechlorination reaction cannot be confirmed or excluded at this time.

### *5.1.2 Methodological Problems*

There are some known methodological issues in the experiments reported above, particularly concerning the calculation of chlorine removal efficiency. For each experiment, mass loss ($m_{loss}$) was determined using the formula presented in Equation (12) where $m_{initial}$ is the initial mass, $m_{final}$ is the final mass, and $m_{vaporized}$ is used to account for the loss of water and organic acids expected due to heating, because $m_{loss}$ should only include the total mass of HCl lost during the reaction. Calculating $m_{vaporized}$ requires making several assumptions about how much water and acid is lost at each temperature. Acid vaporization rates for each temperature were determined based on experiments in which small amounts of acid were heated in a crucible without any salt present.

$$m_{loss} = m_{initial} - m_{final} - m_{vaporized} \quad (12)$$

Problems specific to each system were observed throughout the experimental process. The formic and acetic acid experiments resulted in vigorous boiling of the acids, and there may have been small mass losses that are unaccounted for due to acid droplets being thrown out of the crucible due to the boiling. Oxalic acid presented a slightly different problem, in that there was only partial acid vaporization at high temperatures, and it is suspected that the crystals observed on the sides of the crucibles at the end of many experiments were, in fact, due to oxalic acid crystallizing out of the vapor phase during cooling.

Due to the very small mass differences involved in these thermogravimetric experiments, much of the data are at or near the limit of detection for the laboratory scale used. This problem could be mitigated by increasing the size of the experiments, but scaling these experiments up would require moving them into synthesis glassware systems in order to capture the acid vapor generated and reduce the risk of over-boiling. Several attempts were made to perform larger-scale experiments with a three-bubbler gas capture system (see Figure S4, SI, for an image of this apparatus), with each bubbler having deionized water in it. It was thought that the chlorine removal could be quantified by using the change in pH in each bubbler, but this was found not to be effective because pH measurements cannot distinguish between the HCl vapor and any vaporized acetic, formic, or oxalic acid which may have been carried into the bubblers. Attempts were also made to use ICP-OES to quantify the chlorine in the dissolved reaction product, but due to the very low OES intensity of chlorine and the risk of damaging the argon plasma torch with high-concentration salt solutions, ICP-OES was not able to detect chlorine at low enough concentrations for chlorine quantification.

These problems led to the use of a bubbler with 0.1M $AgNO_3$ during the ERV3 experiments, so that the chlorine removal could be quantified using the AgCl precipitate mass in the bubbler. The results of these experiments were discussed previously and cast significant doubt on the acetic acid thermogravimetric experiments (and by extension the formic acid experiments as well, as formic acid shared many of the potential sources of error). The silver titration results largely support the oxalic acid thermogravimetric results. Due to challenges in capturing all the vapor and condensates produced by these reactions, and with drying and weighing the AgCl precipitate without some portion of it decomposing to metallic Ag, the silver

titration results may underestimate the actual chlorine removal efficiencies during the oxalic acid and ERV3 experiments.

### *5.1.3 Recommendations for Future Organic Acid Dechlorination Experiments*

Several things were learned in this study that could aid future experiments that may be of use in determining the mechanism of these salt + organic acid reactions. Performing the oxalic acid experiments in the presence of water and performing the same experiments with completely dehydrated oxalic acid and salts would provide confirmation on whether water plays a role in this reaction or not. Experiments in larger-scale systems (0.1–1 g salt per experiment) could be conducted in synthesis glassware with acid vapor capture using a system such as an autotitrator to track HCl generation. Experiments on larger sample masses with loose-fitting lids could be used to prevent splattering of solids out of the crucible so that more accurate sample mass readings could be recorded. Additionally, quantitative data on the chloride content of the product salts from the thermogravimetric experiments is very important, which is why ICP-MS was utilized. However, additional techniques could be utilized in the future such as EDS, a Li-detecting technique (e.g., secondary ion mass spectrometry), and a CHNS/O (carbon, hydrogen, nitrogen, sulfur, and oxygen, respectively) analyzer for tracking the residual chemistry in the various products and byproducts.

### *5.1.4 Chlorine Removal of ERV3 Salt*

The initial ERV3 dechlorination experiments indicate that oxalic acid is likely the best candidate of the acids tested, both because high chlorine removal efficiencies have been achieved and because the physical characteristics of oxalic acid (i.e., it is a solid at room temperature, it has a moderate melting temperature) make this reaction preferable to the use of aqueous acids. While the thermogravimetric experiments indicate that oxalic acid dehalogenation increases with temperature, the silver titration experiments indicate that dehalogenation is highest at 150°C and decreases at 200–250°C before plateauing around 250–300°C. This may be the result of the phase change around 200°C, above that temperature the oxalic acid is completely melted and begins to boil. This boiling may have caused a slight positive bias during the high temperature thermogravimetric experiments, resulting in the appearance of higher chlorine

removal efficiencies. The use of solid oxalic acid at 150°C has some advantages beyond high chlorine removal efficiencies, including (1) the oxalic acid does not melt at that temperature, avoiding any issues associated with handling boiling acid, and (2) the solid product is relatively easy to remove from the reaction vessel because it is a crumbly white powder rather than a solid puck (as in the experiments where the oxalic acid melted and re-solidified). Lower temperatures may require a longer heating time. At the 1-g scale, it took upwards of 2 hours for the acid vapor and condensate to be completely removed from the reaction flask at 150°C, but when heated to 300°C, the reaction flask dried completely within 45 min. Further tests could be done to further scale up this reaction, and to determine the relative chlorine removal efficiencies for the component chloride salts in ERV3, as it is not known whether the chlorine removal for the minor components is different than that of the bulk salt.

### *5.2 Glass Waste Form Production*

#### *5.2.1 Glass Durability Testing*

The 7-d PCT-A $NL_B$ and $NL_{Na}$ values for the ERV3-TARS-Q glass were compared to predicted values from Vienna et al.[47] and are illustrated in Figure 8. Here, it can be seen that the $NL_B$ and $NL_{Na}$ values are well below the formulation limit value of 4 $g \cdot m^{-2}$ and EA glass limits reported by Jantzen et al.[57] In addition, these PCT values are also below predicted model values for both cases (Case-1 and Case-2).[47] Similarly, Figure S21 (SI) illustrates the measured ERV3-TARS-Q MCC-1 $NL_{Na}$ values as compared to Parruzot et al.[58] Regarding the MCC-1 testing, the 28-day $NL_{Na}$ for the ERV3-TARS-Q sample values are very comparable to the Case-1 predicted values.

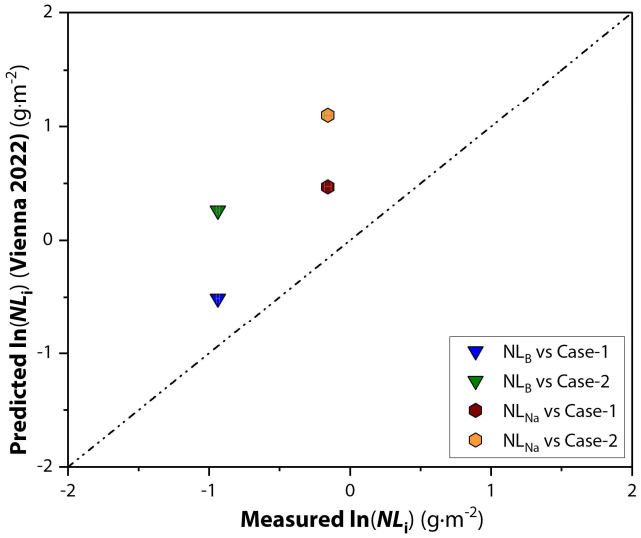


**Figure 8. Normalized loss ($NL_B$, $NL_{Na}$) of the ERV3-TARS-Q glass from the 7-d PCT-A testing compared to Case-1 and Case-2 predicted values using models from Vienna et al.[47]**

### *5.2.2 Crystallinity*

As discussed previously, the primary crystalline phase found in the heat-treated ERV3-TARS-Q glasses appeared to contain $CeO_2$ and $ZrO_2$ and was fit to the $Ce_{0.8}Zr_{0.2}O_2$ phase.[56] This cubic fluorite structure is known to be stable over a long-range order in the stoichiometry found during XRD analysis.[56] Further observations of this structure can be seen in the OM and EDS analyses (see Figure 7 and Figure S20, SI). The formation of aluminosilicates ($KAlSiO_4$ and $KAlSi_2O_6$) in the CCC and lower temperature CF samples ($T$ < 900°C) (Table S12, SI) as silicate crystals are typically noted in glass literature to have adverse effects on glass chemical durability due to the removal of the silica and other glass formers from the glass network, e.g., the formation of nepheline ($NaAlSiO_4$).[59,60] Zircon ($ZrSiO_4$) crystals were also observed to form around idling temperature (950°C) and below. Zircon was also observed in the CCC specimen. However, the slow growth rate,[61] the absence of zircon in the quenched specimen, and the small quantity of zircon detected at idling temperature (≈2.3 mass%) would suggest that the zircon would not contribute a significant negative impact to the glass durability.

### *5.2.3 Processability*

A comparison of the viscosity over temperature of the ERV3-TARS-Q glass is provided in Figure 9, which depicts the measured values falling in the middle of predictions for Case-1 and Case-2. This is consistent with ERV3-TARS-Q representing an average composition between both cases and also shows the accuracy of the predictions. The low viscosity of 1.79 Pa·s at $T_p$ (1150°C) suggests that pourability would not be an issue at that temperature. However, it is important to note that glasses of this viscosity range (> 2 Pa·s) are known to propagate refractory corrosion by penetration into the melter bricks.[62] Lowering the processing temperature to 1050°C would put the glass in a more desirable viscosity range (4.27 Pa·s) but would impact the melt processability of the $CeO_2$.

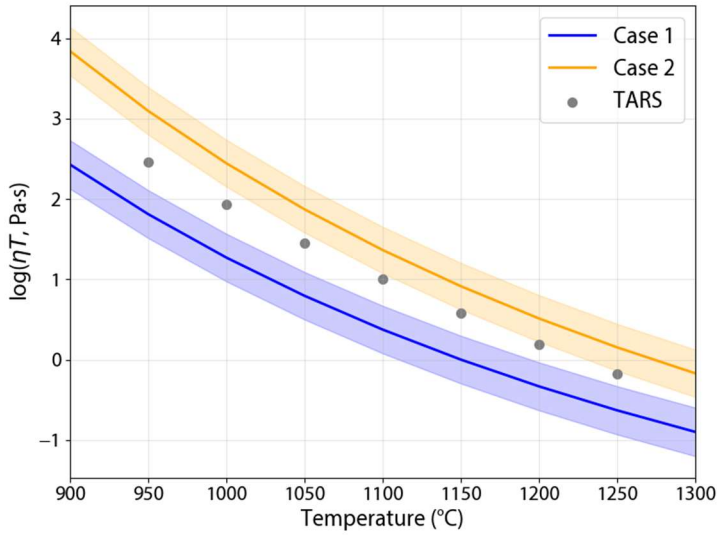


**Figure 9. Viscosity of the ERV3-TARS quenched glass [in terms of log($\eta$), Pa·s] compared to Case-1 and Case-2 predicted values from Vienna et al.[47]**

### *5.3 Electrochemical Salt Waste Form Comparisons*

An effective method for comparing different waste forms for the same process is storage volume (i.e., waste form volume required to immobilize a fixed salt mass, $V_{wf,s}$) versus salt cation loading (mass%, i.e., $m_{sc}$).[23] This can be done using Equation (13) and Equation (14) where $f_{sc,wf}$ denotes the fraction of salt cations in the waste form, $\rho_{wf}$ is the bulk density of the waste form, $\phi$ is the porosity (vol%), $f_{sc,s}$ is the mass

fraction of salt cations in the salt being immobilized or dehalogenated, and $f_{wl,wf}$ is the waste loading in the waste form. The reason for comparing the salt cation loading ($m_{sc}$) and not the full salt loading ($m_s$) is that several different technologies include a dehalogenation step prior to waste form fabrication so comparing them on a full salt basis rather than salt cations only is misleading.

$$V_{wf,s} = \left[\frac{m_{sc}}{(f_{sc,wf})(\rho_{wf})\left(1 - {}^{\phi}/_{100}\right)}\right] \tag{13}$$

$$f_{sc,wf} = (f_{sc,s})(f_{wl,wf}) \tag{14}$$

Based on the calculations described above for past waste forms and the organic acid-derived borosilicate glass waste forms, it is clear by Figure 10 that the organic acid approach (i.e., ERV3-TARS-Q as well as the work by Dong et al.[37]) has some serious advantages over all other technologies that have been explored to date (the $m_{sc}$ value for ERV3-TARS was 23.456 mass%). The other samples included in Figure 10 for comparison include iron phosphate glasses (DPF-1h, DPF-3, DPF-5, DPF5-336),[14] Te-Pb-O glass,[63] glass-bonded sodalite (GBS),[64] and ultrastable H-Y zeolite (USHYZ).[65]

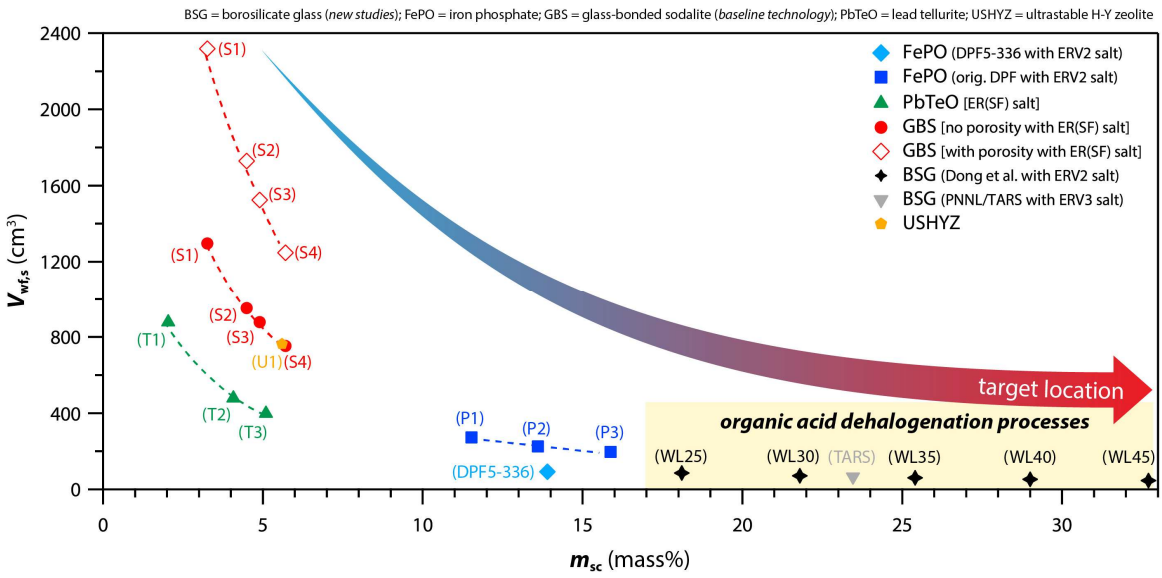


**Figure 10. Summary of waste form volume as a function of salt cation loading in different types of waste forms showing a previously published figure,[23] but with the organic acid dehalogenation work added in the bottom right corner from this work (i.e., TARS) and Dong et al.[37] This includes iron phosphate glasses (DPF-1h,[14] DPF-3,[14] DPF-5,[14] and DPF5-336) Te-Pb-O glass,[63] glass-bonded sodalite (GBS),[64] and ultrastable H-Y zeolite (USHYZ).[65] Reprinted in part with permission from Riley.[23] Copyright 2020 American Chemical Society.**

For reference, TARS is 0.60× the volume of DPF-5 (iron phosphate waste form) for the same amount of starting salt waste and has >2× the total loading of salt cation compared to DPF-5. Also, TARS has 0.72× the volume of DPF5-336 (ERV2 salt) with 1.69× the salt cation loading. It should be noted that the DPF5-336 formulation is the reference iron phosphate waste form that is being studied by the U.S. DOE for chloride salt immobilization.[39,40,66,67] These improvements could be further realized with more advanced glass formulations to continue pushing the waste loading limits higher after initial scoping tests are completed. It is also worth noting that there is a high likelihood of many of the WL# borosilicate glasses produced by Dong et al.[37] failing the chemical durability property requirements based on their notably high alkali loadings compared to the results from this current study where alkali were taken to the maximum possible loading while simultaneously meeting all the other model requirements.

## 6 Summary and Conclusions

Based on a combination of thermogravimetric experiments, $AgNO_3$ titrations, and mass spectrometry, we conclude that oxalic acid provides the greatest chlorine removal at the lowest temperatures of the acids evaluated, followed by formic and acetic acid. Formic acid seems to yield slightly greater chlorine removal than acetic acid based on ICP-MS data, but additional data are needed to confirm this. Oxalic acid generated the highest chlorine removal values for both the simple salt and the ERV3 simulant salt, as confirmed by ICP-MS, but the trends in chlorine removal across the experimental temperature range for the two salts differed. Overall, the highest chlorine removal value obtained in using oxalic acid on the ERV3 simulant salt was at 150°C.

As projections for future studies, the exact mechanism of the dechlorination reaction remains unclear. All experiments reported in this study were performed in ambient air and with hydrated oxalic acid, so it remains unclear what, if any, role water plays in this reaction. Likewise, differences in reactivities between oxalic acid and different chlorine salts also remains unstudied. The differences in the temperature and chlorine removal trends for the simple salt and ERV3 simulant salt may indicate differences in the reactivity of the different salt mixtures. It may be of interest for future experiments to be performed on individual chlorine salts to determine if the reactivity of oxalic acid with these salts varies significantly. Furthermore, based on experience gained from this work, our future study will continue using ICP-MS as the primary analytical method rather than using $AgNO_3$ bubblers or frequent removal from heat for weighing. Chlorine capture in NaOH bubblers can be substituted in for the $AgNO_3$ bubblers to the same effect, and without the risk of unintentionally producing undesirable silver compounds like silver oxalate or silver formate. For the complex simulant (ERV3) experiments, heterogeneities in this salt lead to some uncertainties in the dechlorination efficiency as evidenced by variabilities in both the measured vs expected molar ratios between cations from ICP-MS data and the high KCl content found in the dechlorinated salts with XRD analyses.

Assuming full dechlorination of the ERV3 salt waste and conversion to oxides and carbonates, a glass was formulated based on available glass composition-property models, i.e., a borosilicate glass called TARS. While it is possible that full dechlorination is not required beforehand for a final waste form to meet all of the required product specifications (see Table 9), this was the approach taken for the current study. The TARS glass was melted, quenched, and then several properties were studied. The TARS waste form results are summarized in Table 9 and compared with the predicted values presented in Table S3 (SI), including $\eta$, durability (i.e., MCC-1, PCT), $\rho$, $T_g$, and $T_L$.

**Table 9. Measured values for $\eta$, PCT (i.e., $NL_B$ and $NL_{Na}$ for 7-d test), MCC-1 (i.e., $NL_{Na}$ for 28-d test), $\rho$, $T_g$, and $T_L$ along with predicted properties for Case-1 and Case-2 compositions based on models (with references to the models). Note that $T_p$ is the processing temperature (1150°C). The relevant sections for where these measurements and data are discussed within the paper are provided.**

| Property | Measured Values | Predicted Values | | Model refs. | Relevant Sections |
|---|---|---|---|---|---|
| | ERV3-TARS-Q | Case-1 | Case-2 | | |
| $\eta$ at $T_p$ (Pa·s) | 1.79 | 1.0 | 2.5 | Vienna et al.[47] | 3.2.5, 4.2, 5.2.3, SI |
| PCT ($NL_B$) (7-d) ($g \cdot m^{-2}$) | 0.26 ± 0.01 | 0.6 | 1.6 | Vienna et al.[47] | 3.2.4, 4.2, 5.2.1, SI |
| PCT ($NL_{Na}$) (7-d) ($g \cdot m^{-2}$) | 0.85 ± 0.02 | 1.3 | 3.0 | Vienna et al.[47] | 3.2.4, 4.2, 5.2.1, SI |
| MCC-1 ($NL_{Na}$) (28-d) ($g \cdot m^{-2}$) | 11.43 | 11.99 | 17.40 | Parruzot et al.[58] | 3.2.4, 4.2, 5.2.1, SI |
| $\rho$ ($g \cdot cm^{-3}$) | 2.721 | 2.61 | 2.73 | Vienna et al.[68] | 3.2.5, 4.2 |
| | 2.721 | 2.70 | 2.77 | Vienna et al.[69] | 3.2.5, 4.2 |
| $T_g$ (°C) | 446.2 | 438 | 474 | George et al.[70] | 3.2.5, 4.2, SI |
| $T_L$ (°C) ($Ce_{0.8}Zr_{0.2}O_2$) | 1154 | – | – | – | 3.2.5, 4.2, 5.2.2, SI |

The measured $\eta$ and $\rho$ values for the ERV3-TARS glass fall in between the two different predictions (Case-1 and Case-2). Comparable $NL_i$ values from chemical durability testing show that the TARS formulation performed even better than the predicted models. The $NL_B$ and $NL_{Na}$ values from the PCT-A test were well below both case models, and the 28-day $NL_{Na}$ values from the MCC-1 test were slightly below the predicted Case-1 values. The quenched glass was mostly amorphous, with some undissolved $CeO_2$. The primary crystalline phase found in the isothermally heat-treated glass was a ceria-stabilized cubic zirconia phase ($Ce_{0.8}Zr_{0.2}O_2$), which had a measured $T_L$ value of 1154°C. Additional low temperature

crystalline phases such as various potassium-aluminosilicates, zirconosilicates, and potassium-zirconosilicates were observed below specific temperature points and in the CCC specimen.

Waste forms produced using organic acid dechlorination methods have the potential to drastically improve salt cation waste loadings over current waste forms being explored, which include glass-bonded sodalite ceramic waste forms and phosphate waste forms produced using phosphate-based dechlorination processes (i.e., ADP, $H_3PO_4$). Additional work could be done to push the waste loading even higher than what was demonstrated in this study for TARS, which was a waste loading of 23.46 mass% salt cations or 30.82 mass% on an oxide basis.

## 7 Author Information


**Corresponding authors**

Brian J. Riley – Pacific Northwest National Laboratory, Richland, WA 99334, United States; email: brian.riley@pnnl.gov

Xiaofeng Guo – Washington State University, Pullman, WA 99164, United States: email: x.guo@wsu.edu

**Authors**

Jared M. Oshiro – Pacific Northwest National Laboratory, Richland, WA 99334, United States

Hannah Hallikainen – Washington State University, Pullman WA 99164, United States

Xiaonan Lu – Pacific Northwest National Laboratory, Richland, WA 99334, United States

Bhargav Iyer – Washington State University, Pullman WA 99164, United States

Bryn Merrill – Washington State University, Pullman WA 99164, United States

Vitaliy Goncharov – Washington State University, Pullman WA 99164, United States

Jesse Westman – Pacific Northwest National Laboratory, Richland, WA 99334, United States

Martin Liezers – Pacific Northwest National Laboratory, Richland, WA 99334, United States

Jaime L. George – Pacific Northwest National Laboratory, Richland, WA 99334, United States

Benjamin Parruzot – Pacific Northwest National Laboratory, Richland, WA 99334, United States

Jonathan S. Evarts – Pacific Northwest National Laboratory, Richland, WA 99334, United States

John D. Vienna – Pacific Northwest National Laboratory, Richland, WA 99334, United States

John S. McCloy – Washington State University, Pullman WA 99164, United States

## 8 Associate Content

The Supporting Information is available free of charge via the Internet at https://pubs.acs.org/.

Background on experimental approach, details and results for dechlorination experiments, glass formulation details, heat treatment profile information, ICP-MS data for dechlorination experiments, XRD data for dehalogenation experiments, chemical durability testing data, differential scanning calorimetry data, viscosity data, liquidus temperature data for ERV3-TARS-Q, viscosity data, optical microscopy data, and XRD data for TARS specimens (Q, CCC, and $T_L$).

## 9 Acknowledgements

This work was funded through the U.S. Department of Energy Office of Nuclear Energy through the Material Recovery and Waste Form Development Campaign under the Nuclear Fuel Cycle and Supply Chain Program. Pacific Northwest National Laboratory (PNNL) is operated by Battelle Memorial Institute for the DOE under contract DE-AC05-76RL01830. Authors would like to thank Jacqueline Ferrer (PNNL), Miroslava Peterson (PNNL), Joelle Reiser (PNNL), Jarrod Crum (PNNL), Jose Marcial (PNNL), Jess Rigby (PNNL), Ian Burch (PNNL), and Megan Miller (PNNL) for their assistance with glass characterization and testing, and Yiyuan Jia (WSU) for his assistance with setting up initial testing of dechlorination.

## 10 References

(1) Laidler, J. J.; Battles, J. E.; Miller, W. E.; Ackerman, J. P.; Carls, E. L. Development of pyroprocessing technology. *Prog. Nucl. Energy* **1997**, *31*, 131-140.

(2) Simpson, M. F.; Goff, K. M.; Johnson, S. G.; Bateman, K. J.; Battisti, T. J.; Toews, K. L.; Frank, S. M.; Moschetti, T. L.; O'Holleran, T. P.; Sinkler, W. A Description of the Ceramic Waste Form Production Process from the Demonstration Phase of the Electrometallurgical Treatment of EBR-II Spent Fuel. *Nucl. Technol.* **2001**, *134*, 263-277.

(3) LeBlanc, D. Molten salt reactors: A new beginning for an old idea. *Nucl. Eng. Des.* **2010**, *240*, 1644-1656.

(4) Serp, J.; Allibert, M.; Beneš, O.; Delpech, S.; Feynberg, O.; Ghetta, V.; Heuer, D.; Holcomb, D.; Ignatiev, V.; Kloosterman, J. L.; Luzzi, L.; Merle-Lucotte, E.; Uhlíř, J.; Yoshioka, R.; Zhimin, D. The molten salt reactor (MSR) in generation IV: Overview and perspectives. *Prog. Nucl. Energy* **2014**, *77*, 308-319.

(5) Riley, B. J.; McFarlane, J.; DelCul, G. D.; Vienna, J. D.; Contescu, C. I.; Forsberg, C. W. Molten salt reactor waste and effluent management strategies: A review. *Nucl. Eng. Des.* **2019**, *345*, 94-109.

(6) Aghili Nasr, M.; Zolfaghari, A.; Akbari, R.; Cammi, A.; Amirkhosravi, S. Neutronic and fuel cycle performance analysis of fluoride and chloride fuels in Molten Salt Fast Reactor (MSFR). *Nucl. Eng. Des.* **2023**, *413*, 112506.

(7) Ackerman, J. P.; Johnson, T. R.; Chow, L. S. H.; Carls, E. L.; Hannum, W. H.; Laidler, J. J. Treatment of Wastes in the IFR Fuel Cycle. *Prog. Nucl. Energy* **1997**, *31*, 141-154.

(8) Davis, L.; Hania, R.; Boomstra, D.; Rossouw, D.; Charpin-Jacobs, F.; Uhlir, J.; Maracek, M.; Beckers, H.; Riedel, S. Radiolytic Production of Fluorine Gas from MSR Relevant Fluoride Salts. *Nucl. Sci. Eng.* **2023**, *197*, 633-646.

(9) Del Cul, G. D.; Icenhour, A. S.; Simmons, D. W. *Prototype Tests for the Recovery and Conversion of $UF_6$ Chemisorbed in NaF Traps for the Molten Salt Reactor Remediation Project* ORNL/TM-2000/92, Oak Ridge National Laboratory, Oak Ridge, TN, 2000.

(10) Del Cul, G. D.; Icenhour, A. S.; Simmons, D. W.; Trowbridge, L. D.; Williams, D. F.; Toth, L. M.; Dai, S. Overview of the recovery and processing of $^{233}U$ from the Oak Ridge molten salt reactor experiment (MSRE) remediation activities. In Proc. Global 2001 International Conference on Back-End of the Fuel Cycle: From Research to Solutions. **2001**; pINIS-FR-1169.

(11) Sheppard, S. C.; Johnson, L. H.; Goodwin, B. W.; Tait, J. C.; Wuschke, D. M.; Davison, C. C. Chlorine-36 in nuclear waste disposal—1. Assessment results for used fuel with comparison to $^{129}I$ and $^{14}C$. **1996**, *16*, 607-614.

(12) Riley, B. J.; Turner, J. R.; McFarlane, J.; Chong, S.; Carlson, K.; Matyáš, J. Iodine solid sorbent design: a literature review of the critical criteria for consideration. *Mater. Adv.* **2024**, *5*, 9515-9547.

(13) He, L.-Y.; Li, G.-C.; Xia, S.-P.; Chen, J.-G.; Zou, Y.; Liu, G.-M. Effect of $^{37}$Cl enrichment on neutrons in a molten chloride salt fast reactor. *Nucl. Sci. Tech.* **2020**, *31*, 27.

(14) Riley, B. J.; Peterson, J. A.; Vienna, J. D.; Ebert, W. L.; Frank, S. M. Dehalogenation of electrochemical processing salt simulants with ammonium phosphates and immobilization of salt cations in an iron phosphate glass waste form. *J. Nucl. Mater.* **2020**, *529*, 151949.

(15) *Waste Forms Technology and Performance: Final Report*; National Research Council, The National Academies Press: Washington, DC, 2011, 978-0-309-18733-6.

(16) Petrov, V. A.; Ojovan, M. I.; Yudintsev, S. V. Material Aspect of Sustainable Nuclear Waste Management. *Sustain.* **2023**, *15*, 11934.

(17) Hrma, P. R. *Retention of Halogens in Waste Glass*, PNNL-19361, Pacific Northwest National Laboratory, Richland, WA, 2010.

(18) Riley, B. J.; Schweiger, M. J.; Kim, D.-S.; Lukens Jr, W. W.; Williams, B. D.; Iovin, C.; Rodriguez, C. P.; Overman, N. R.; Bowden, M. E.; Dixon, D. R.; Crum, J. V.; McCloy, J. S.; Kruger, A. A. Iodine solubility in a low-activity waste borosilicate glass at 1000 °C. *J. Nucl. Mater.* **2014**, *452*, 178-188.

(19) Riley, B. J.; Rieck, B. T.; McCloy, J. S.; Crum, J. V.; Sundaram, S. K.; Vienna, J. D. Tellurite glass as a waste form for mixed alkali-chloride waste streams: candidate materials selection and initial testing. *J. Nucl. Mater.* **2012**, *424*, 29-37.

(20) Gardner, L.; Harward, A.; Howard, J.; Fredrickson, G.; Yoo, T.-S.; Simpson, M.; Carlson, K. Deliquescence of Eutectic LiCl-KCl Diluted with NaCl for Interim Waste Salt Storage. *Nucl. Technol.* **2022**, *208*, 310-317.

(21) Harward, A.; Elliott, C.; Shaltry, M.; Carlson, K.; Yoo, T.-S.; Fredrickson, G.; Patterson, M.; Simpson, M. F. Synthesis and characterization of super occluded LiCl-KCl in zeolite-4A as a chloride salt waste form intermediate. *J. Nucl. Mater.* **2024**, *588*, 154816.

(22) Riley, B. J. *Electrochemical Salt Waste Form Development: A Comparison with Iron Phosphate Glass*, PNNL-28745, Pacific Northwest National Laboratory, Richland, WA, 2019.

(23) Riley, B. J. Electrochemical salt wasteform development: A review of salt treatment and immobilization options. *Ind. Eng. Chem. Res.* **2020**, *59*, 9760-9774.

(24) Riley, B. J.; Chong, S. Glass waste form options for rare-earth fission products from electrochemical reprocessing. *J. Non-Cryst. Solids* **2020**, *545*, 120161.

(25) Riley, B. J.; Chong, S.; Lonergan, C. E. Dechlorination Apparatus for Treating Chloride Salt Wastes: System Evaluation and Scale-Up. *ACS Omega* **2021**, *6*, 32239-32252.

(26) Murray, P.; Werth, H.; Sullivan, S.; Riley, B. J.; Simpson, M.; Lonergan, C.; Carlson, K. Phosphate-based dechlorination of electrorefiner salt waste using a phosphoric acid precursor. *ACS Omega* **2024**, *9*, 19395-19400.

(27) Evarts, J. S.; Riley, B. J.; Lonergan, C.; Harris, M. S.; Bai, J.; Bohannan, E.; Iheanyichukwu, A.; Chong, S.; McCloy, J. S. Synergy in Materials: Leveraging Phosphosilicate Waste Forms for Electrochemical Salt Waste. *ACS Sustainable Resour. Manage.* **2024**, *2*, 514-523.

(28) Siemer, D. D. Improving the integral fast reactor's proposed salt waste management system. *Nucl. Technol.* **2012**, *178*, 341-352.

(29) Donze, S.; Montagne, L.; Palavit, G. Thermal conversion of heavy metal chlorides ($PbCl_2$, $CdCl_2$) and alkaline chlorides (NaCl, KCl) into phosphate glasses. *Chem. Mater.* **2000**, *12*, 1921-1925.

(30) Ebert, W. L. *Testing to Evaluate the Suitability of Waste Forms Developed for Electrometallurgically-Treated Spend Sodium-Bonded Nuclear Fuel for Disposal in the Yucca Mountain Repository*, ANL-05/43, Argonne National Laboratory-East, Argonne, IL, 2005.

(31) Riley, B. J.; Vienna, J. D.; Ebert, W. L. *Road Map for Developing Iron Phosphate Waste Forms for Salt Wastes*, PNNL-30998, ANL/CFCT-20/44, Pacific Northwest National Laboratory, Richland, WA, 2021.

(32) Riley, B. J.; Chong, S. Dehalogenation reactions between halide salts and phosphate compounds. *Front. Chem.* **2022**, *10*, 976781.

(33) Vitart, A.-L.; Haidon, B.; Arab-Chapelet, B.; Rivenet, M.; Bisel, I.; Pochon, P.; Roussel, P.; Grandjean, S.; Abraham, F. From Nd(III) and Pu(III) Oxalates to Oxides: Influence of Nitrilotris(methylenephosphonic acid) on Chemical Composition, Structure, and Morphology. *Cryst. Growth Des.* **2017**, *17*, 4715-4725.

(34) Syed, S.; Buddolla, V.; Lian, B. Oxalate Carbonate Pathway-Conversion and Fixation of Soil Carbon-A Potential Scenario for Sustainability. *Front. Plant Sci.* **2020**, *11*, 591297.

(35) Yeh, P. Y.; Lin, L. C.; Yang, S. S.; Chen, S. M. Differentiation of Organic Acids and Phenols by Heating with Metal Halides. *Anal. Chem.* **1962**, *34*, 990-993.

(36) Lin, L. C.; Yeh, P.-Y. The Effect of Water on the Reaction of Metal Halides with Organic Acids at Higher Temperatures. *J. Chin. Chem. Soc.* **1961**, *8*, 210-219.

(37) Dong, Y.; Xu, K.; Jia, Z.; Niu, C.; Xu, D. Dechlorination and vitrification of electrochemical processing salt waste. *J. Nucl. Mater.* **2022**, *567*, 153833.

(38) Riley, B. J.; Canfield, N. L.; Peterson, M.; George, J. L.; Chong, S.; Crum, J. V. *Crystalline versus Glassy Nature of Iron Phosphate Waste Forms Subjected to Different Slow Cooling Curves*, PNNL-34917, Pacific Northwest National Laboratory, Richland, WA, 2023.

(39) Riley, B. J.; Chong, S.; Nienhuis, E. T. *Canister Centerline Cooling Experiments for DPF5-336 Reference Material Made with ERV3b Salt Simulant*, PNNL-33802, Pacific Northwest National Laboratory, Richland, WA, 2023.

(40) Riley, B. J.; Chong, S.; Peterson, M.; Nienhuis, E. T. *Aluminophosphate Waste Forms for Immobilizing Cations from Electrochemical Salt Wastes*, PNNL-33906, Pacific Northwest National Laboratory, Richland, WA, 2023.

(41) Stariha, S. A.; Ebert, W. L. *Durability Assessments of Quenched and Slow-Cooled Iron Phosphate Waste Form Materials*, ANL/CFCT-23/24, Argonne National Laboratory, Lemont, IL, 2023.

(42) Tolman, D. D.; Riley, B. J. *Conceptual Design of a Salt Dechlorination and Vitrification Apparatus (DeVA)*, INL/RPT-23-72319, PNNL-34755, Idaho National Laboratory, Idaho Falls, ID, 2023.

(43) Rankin, W. N.; O'Rourke, P. E.; Soper, P. D.; Cosper, M. B.; Osgood, B. C. *Evaluation of Corrosion and Deposition in the 1941 Melter*, DPST-82-231, E. I du Pont de Nemours & Co, Savannah River Laboratory, Aiken, SC, 1982.

(44) Fox, K. M. *Crystallization in High Level Waste (HLW) Glass Melters: Operational Experience from the Savannah River Site*, SRNL-STI-2013-00724, Savannah River National Laboratory, Aiken, SC, 2014.

(45) Matyáš, J.; Sevigny, G.; Venarsky, J.; Davis, J.; Lukins, C.; Lang, J.; Edwards, M.; Stewart, C.; Sannoh, S.; Veldman, T.; Phillips, N.; Fischer, C. *Evaluation of Crystal Accumulation in HighLevel Waste Glasses with Research-Scale Melter* PNNL-27419, EWG-RPT-018, Pacific Northwest National Laboratory, Richland, WA, 2018.

(46) Vienna, J. D.; Crum, J. V. Non-linear effects of alumina concentration on Product Consistency Test response of waste glasses. *J. Nucl. Mater.* **2018**, *511*, 396-405.

(47) Vienna, J. D.; Heredia-Langner, A.; Cooley, S. K.; Holmes, A. E.; Kim, D. S.; Lumetta, N. A. *Glass property-composition models for support of Hanford WTP LAW facility operation* PNNL-30932, Rev 2, Pacific Northwest National Laboratory, Richland, WA, 2022.

(48) Lu, X.; Sargin, I.; Vienna, J. D. Predicting nepheline precipitation in waste glasses using ternary submixture model and machine learning. *J. Am. Ceram. Soc.* **2021**, *104*, 5636-5647.

(49) ASTM C1285-21, ASTM C1285-21, Standard Test Methods for Determining Chemical Durability of Nuclear, Hazardous, and Mixed Waste Glasses and Multiphase Glass Ceramics: The Product Consistency Test (PCT), American Society for Testing and Materials International, ASTM International Book of Standards Volume 12.01, West Conshohocken, PA, 2021.

(50) Riley, B. J.; Chong, S. Effects of composition and canister centerline cooling on microstructure, phase distribution, and chemical durability of dehalogenated iron phosphate waste forms. *J. Non-Cryst. Solids* **2021**, *579*, 121319.

(51) ASTM C1220-21, ASTM C1220-21, Standard Test Method for Static Leaching of Monolithic Waste Forms for Disposal of Radioactive Waste, American Society for Testing and Materials International, ASTM International Book of Standards Volume 12.01, West Conshohocken, PA, 2021.

(52) ASTM D1193-99e1, Standard Specification for Reagent Water, American Society for Testing and Materials International, ASTM International Book of Standards Volume 11.01, West Conshohocken, PA, 2017.

(53) Crum, J. V.; Edwards, T. B.; Russell, R. L.; Workman, P. J.; Schweiger, M. J.; Schumacher, R. F.; Smith, D. E.; Peeler, D. K.; Vienna, J. D. DWPF Startup Frit Viscosity Measurement Round Robin Results. *J. Am. Ceram. Soc.* **2012**, *95*, 2196-2205.

(54) ASTM C1720-21, ASTM C1720-21, Standard Test Method for Determining Liquidus Temperature of Waste Glasses and Simulated Waste Glasses, American Society for Testing and Materials International, ASTM International Book of Standards Volume 12.01, West Conshohocken, PA, 2021.

(55) SRM-674b, SRM-674b. X-Ray Powder Diffraction Intensity Set (Quantitative Powder Diffraction Standard), National Institute of Standards and Technology, Gaithersburg, MD, 2018.

(56) Singh, H.; Sharma, S. K.; Kulriya, P. K. Electronic excitation driven structural evolution in $Ce_{0.8}Zr_{0.2}O_2$. *Ceram. Int.* **2023**, *49*, 7946-7955.

(57) Jantzen, C. M.; Bibler, N. E.; Beam, D. C.; Crawford, C. L.; Pickett, M. A. *Characterization of the Defense Waste Processing Facility (DWPF) Environmental Assessment (EA) Glass Standard Reference Material (U)*, WSRC-TR-92-346, Rev.1, Savannah River Site, Aiken, SC, 1993.

(58) Parruzot, B.; Reiser, J. T.; Lu, X.; Crum, J. V.; Reyes, R. A.; Finucane, K. G.; Witwer, K. S.; Abeta, S.; Yoshioka, M.; Vienna, J. D. Durability evaluation of glasses to immobilize Fukushima (1F) secondary waste using ASTM C1220 (MCC-1) testing. *J. Non-Cryst. Solids X* **2023**, *19*, 100197.

(59) Fox, K.; Edwards, T. G.; Peeler, D. K. Control of Nepheline Crystallization in Nuclear Waste Glass. *Int. J. Appl. Ceram. Technol.* **2008**, *5*, 666-673.

(60) McCloy, J. S.; Schweiger, M. J.; Rodriguez, C. P.; Vienna, J. D. Nepheline Crystallization in Nuclear Waste Glasses: Progress Toward Acceptance of High-Alumina Formulations. *Int. J. Appl. Glass Sci.* **2011**, *2*, 201-214.

(61) Riley, B.; Rosario, J.; Hrma, P.; Vienna, J. Effect of crystallization on high-level waste glass corrosion. In Proc. Ceram. Trans. **2002**; Vol. 132 p257-265.

(62) Hrma, P.; Piepel, G.; Schweiger, M.; Smith, D.; Kim, D.; Redgate, P.; Vienna, J.; Lopresti, C.; Simpson, D.; Peeler, D.; Langowski, M. *Property/Composition Relationships for Hanford High-Level Waste Glasses Melting at 1150°C Volume 2: Chapters 12-16 and Appendices A-K*, PNNL-10359, Pacific Northwest National Laboratory, Richland, WA, 1994.

(63) Riley, B. J.; Kroll, J. O.; Peterson, J. A.; Pierce, D. A.; Ebert, W. L.; Williams, B. D.; Snyder, M. M. V.; Frank, S. M.; George, J. L.; Kruska, K. Assessment of lead tellurite glass for immobilizing electrochemical salt wastes from used nuclear fuel reprocessing. *J. Nucl. Mater.* **2017**, *495*, 405-420.

(64) Riley, B. J.; Vienna, J. D.; Frank, S. M.; Kroll, J. O.; Peterson, J. A.; Canfield, N. L.; Zhu, Z.; Zhang, J.; Kruska, K.; Schreiber, D. K. Glass binder development for a glass-bonded sodalite ceramic waste form. *J. Nucl. Mater.* **2017**, *489*, 42-63.

(65) Gardner, L. D.; Wasnik, M. S.; Riley, B. J.; Chong, S.; Simpson, M. F.; Carlson, K. L. Synthesis and characterization of sintered H-Y zeolite-derived waste forms for dehalogenated electrorefiner salt. *Ceram. Int.* **2020**, *46*, 17707–17716.

(66) Ebert, W. L.; Fortner, J. A. *Analyses of Iron Phosphate Glasses for Dehalogenated Salt Waste*, ANL/CFCT-19/5, Argonne National Laboratory, Lemont, IL, 2019.

(67) Evarts, J. S.; Riley, B. J.; Carlson, K.; Simpson, M. Phosphate-Based Approaches for Dechlorination and Treatment of Salt Waste from Electrochemical Processing of Used Nuclear Fuel: A Perspective on Recent Work. *in preparation for Ind. Eng. Chem. Res.* **2025**.

(68) Vienna, J. D.; Fluegel, A.; Kim, D. S.; Hrma, P. R. *Glass property data and models for estimating high-level waste glass volume* PNNL-18501, Pacific Northwest National Laboratory, Richland, WA, 2009.

(69) Vienna, J. D.; Kim, D. S.; Hrma, P. R. *Database and Interim Glass Property Models for Hanford HLW and LAW Glasses* PNNL-14060, Pacific Northwest National Laboratory, Richland, WA, 2002.

(70) George, J. L.; Ferkl, P.; Marcial, J.; Jin, T.; Hrma, P.; Kruger, A. A. Glass transition temperature of low-activity waste nuclear glasses. *Int. J. Appl. Glass Sci.* **2023**, *14*, 399-407.